Heating Glass-Forming Materials

by

Time Dependent Electric Fields

by

Ullas Pathak

A Thesis Presented in Partial Fulfillment
of the Requirements for the Degree
Master of Science

Approved July 2012 by the
Graduate Supervisory Committee:

Ranko Richert, Co-Chair
Lenore Dai, Co-Chair
David Nielsen

ARIZONA STATE UNIVERSITY

December 2012

ABSTRACT

The disordered nature of glass-forming melts results in two features for its dynamics i.e. non-Arrhenius and non-exponential behavior. Their macroscopic properties are studied through observing spatial heterogeneity of the molecular relaxation. Experiments performed in a low-frequency range tracks the flow of energy in time on slow degrees of freedom and transfer to the vibrational heat bath of the liquid, as is the case for microwave heating. High field measurements on supercooled liquids result in generation of fictive temperatures of the absorbing modes which eventually result in elevated true bath temperatures. The absorbed energy allows us to quantify the changes in the 'configurational', real sample, and electrode temperatures. The slow modes absorb energy on the structural relaxation time scale causing the increase of configurational temperature resulting in the rise of dielectric loss. Time-resolved high field dielectric relaxation experiments show the impact of 'configurational heating' for low frequencies of the electric field and samples that are thermally clamped to a thermostat. Relevant thermal behavior of monohydroxy alcohols is considerably different from the cases of simple non-associating liquids, due to their distinct origins of the prominent dielectric loss. Monohydroxy alcohols display very small changes due to observed nonthermal effects without increasing sample temperature. These changes have been reflected in polymers in our measurements.

ACKNOWLEDGMENTS

I would like to thank Dr. Ranko Richert for his inspiration, support and esteemed guidance. Dr. Richert is not only a renowned scientist but also a great mentor and teacher. His zeal towards research has inspired me to learn and have a better perspective, influencing me to become a researcher like him one day. I will also like to thank my committee members Dr. Lenore Dai and Dr. David Nielsen for their timely support and advice towards research and my thesis work.

I dedicate this thesis to my grandmother Shrimati Savitri Tripathi and my parents. Their support and love has made me what I am today. I would like to thank the post-docs in my group Dr. Zhen Chen and Dr. Lokendra Singh. They helped me to develop intellectually and provided me an insight on dielectrics with their experience. My discussions with them have helped me to gain a better understanding. I will also like to thank the other members in my group Subarna Samanta, Soham Roy and Shobeir Mazinani for their support.

Last but not the least I will like to thank all my friends for being there for me in good and bad times, and making these two years wonderful.

TABLE OF CONTENTS

Page

LIST OF FIGURES

Chapter 1

INTRODUCTION

1.1 Supercooled Liquids

Glass being one of the most widely used materials has unresolved problems related to understanding it. It is sometimes difficult to say, is glass a liquid or a solid? Often it has been confused as a liquid due to disordered arrangement of glass panes in old churches as they were thicker at the bottom and became slimmer at the top while not in liquid form. When a liquid is cooled from a high temperature it crystallizes and forms a solid. Freezing is related by a release of heat known as the heat of fusion. In condensed matter physics there has been a limiting factor for the study of glass and glass-forming melts. Thermodynamically there is a separate terminology as glass but not many accept this terminology in commercialized world. It has been studied over the years that most of the solids have a crystalline structure at microscopic level. Solid state chemistry says that heating a solid provides energy to the molecules to vibrate about their position in a lattice. In a crystal the molecules are arranged in a regular lattice. Heating above a solid above the melting temperature T_m, causes the crystal to break down and initiate the flow of molecules. The difference between solid and liquid is met by the first order phase transition i.e. a discontinuous change of materialistic properties as density occurs in this transition. Viscosity is the resistance to flow. A liquid is marked by viscosity which increases by decreasing the temperature. When the rate of cooling is monitored to the limiting point of the liquid, the transition is influenced by viscosity while further decreasing the rate of cooling

crystallizes the liquid. At a certain temperature the timescale of molecular rearrangements becomes longer compared to the timescale of experimental observation. There is a sharp distinction between the solid and liquid phase in which viscosity plays a role and prevents the molecules from crystallization. Release of heat during freezing occurs at the melting temperature T_m. Glass has been manufactured in various ways, one of which is cooling a liquid below its melting temperature. If a liquid does not crystallize below its melting temperature T_m, it is called a supercooled liquid.

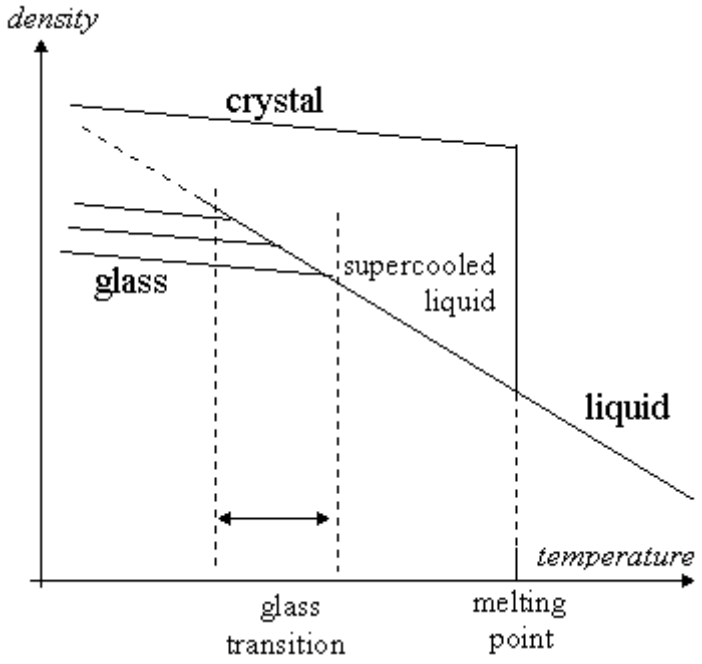

Figure 1.1: Glass transition temperature and regime of supercooled liquid.

When cooling a liquid the crystallization occurs at the melting temperature but after attaining a supercooled state it often remains a liquid. The inability of nuclei to grow to microscopic size due to increase in viscosity hence preventing

crystallization causing the liquid to form a supercooled liquid which further becomes an amorphous solid, and hence is known as glass. Glass has a disordered arrangement but cohesion to maintain rigidity causing the molecules in glass to be rigidly bound. Thermodynamics has a significantly role in the transition from liquid to solid as a crystal is energetically more favorable than the liquid below melting point. Transition from supercooled liquid to formation of glass is kinetic. Due to disorderly nature, the glassy state does not have enough kinetic energy to overcome the potential barriers for movement of molecules past one another. Glass and supercooled liquids are in a metastable state unlike crystalline solids which is a real thermodynamically stable phase. A second order phase transition distinguishes the glassy and the supercooled liquid state. In contrast to the phase transition from liquid to solid this transition is not accompanied by a discontinuous change in density and latent heat of fusion. Supercooled liquid and glassy state can be differentiated by the thermal expansivity and heat capacity of the material undergoing a change in this transition. The temperature at which this transition occurs is known as the glass transition temperature. Rate of cooling decides the glass transition temperature which varies for different materials and has a threshold. Rise of viscosity causes the liquid to develop as thick syrup and hence attain an amorphous state. Theoretically as well as in principle it has been proved that a glass could undergo a transition into a crystallized solid any time, the sole reason that old glass devitrifies due to presence of impurities. Molecular physics defines four levels of molecular arrangement:

Crystalline Solids: Molecules are ordered in a regular lattice.

Fluids: Molecules are disordered and have no rigidity.

Glass: Molecules are disordered and are rigidly bound.

Quasi-crystal: Molecular motion is that of between a crystal and glass.

1.2 Dielectric Mechanisms

Several dielectric mechanisms or polarization effects can happen in a material, which contribute to its overall permittivity. Charge carriers in a dielectric material can be displaced by an electric field. The charges become polarized to compensate for the electric field such that the positive and negative charges move in opposite directions. The behavior of dielectric properties as a function of frequency in insulating materials is governed by dielectric polarization effects. The polarization phenomena in a dielectric material over a wide time scale can be seen in Figure 1.2 and it can be observed that different polarization mechanisms dominate over different frequency ranges.

$$\mathbf{P} = \varepsilon\varepsilon_0\mathbf{E} \qquad (1.1)$$

where **P** describes the dielectric displacement originated by the response of the sample to an external field **E** and ε_0 is the dielectric permittivity of vacuum and ε the complex dielectric function or dielectric permittivity.

1.3 Dielectric Spectroscopy

Each dielectric mechanism is centered on its characteristic frequency (angular frequency ω), which is the reciprocal of the characteristic time of the process (τ) i.e. $\tau = 1/\omega$ and $\omega = 2\pi\nu$ (ν is the frequency). In general, dielectric mechanisms

can be divided into relaxation and resonance processes. Relaxation mechanisms are relatively slow compared to resonant electronic transitions or molecular vibrations, which usually have frequencies above 10^{12} Hz. Resonant electronic transitions have an oscillatory time domain response in which the current changes time periodically. Dielectric relaxation is the result of the movement of dipoles and electric charges due to an applied alternating field. However, relaxation mechanisms are based on polarization mechanisms and hence slower because of which they occur at lower frequencies. As frequency increases, the slow mechanisms drop out in turn, leaving the faster ones to contribute to ε. The loss factor will correspondingly peak at each critical frequency. The magnitude and "cutoff frequency" of each mechanism is unique for different materials. Figure 1.2 shows relaxation and resonance phenomena.

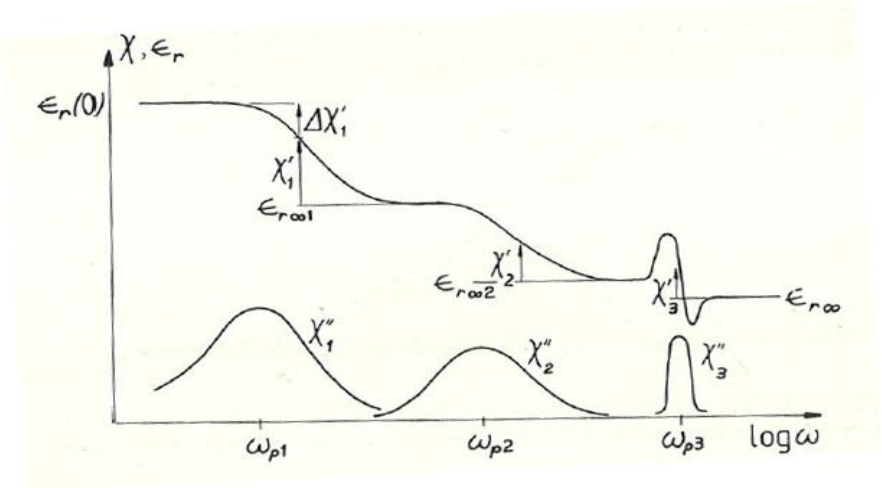

Figure 1.2: Different relaxation and resonance processes

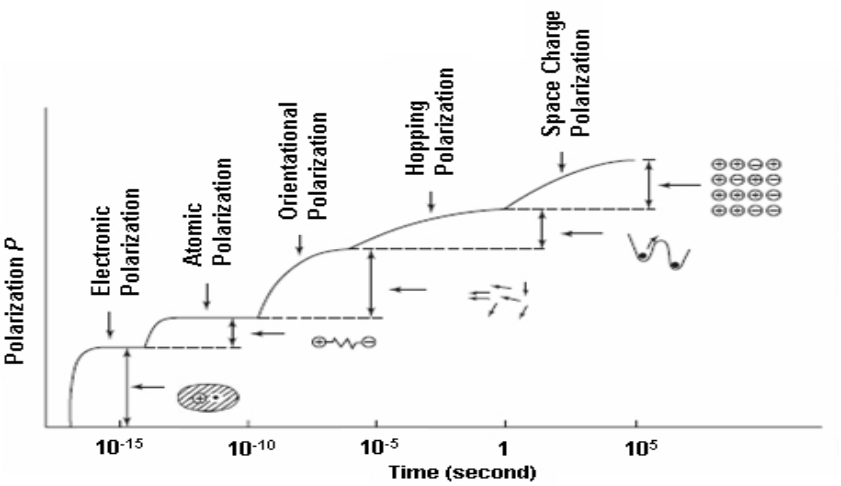

Figure1.3: Different polarization phenomena occurring in a solid dielectric

1.4 Polarization

Electronic and atomic polarizations

Electronic polarization occurs in all atoms even with dipoles when an electric field displaces the nucleus with respect to the electrons that surround it. Atomic polarization occurs when adjacent positive and negative ions are stretched relative to the nuclei under an applied electric field. For many solids, these are the dominant polarization mechanisms at microwave frequencies, although the actual resonance occurs at a much higher frequency [1]. The resonant frequency is identified by a resonant response in ε' and a peak of maximum absorption in ε". Below resonance frequency, the electronic and atomic mechanisms contribute only a small constant amount to ε^* and are almost lossless as $\varepsilon^* = (n^*)^2$ where n^* is the complex index of refraction.. Above resonance, the contribution from these mechanisms disappears.

Dipolar or orientational polarization

Orientational polarization is a classical type of polarization and it refers to polar molecules floating freely in a dielectric and for simplicity it was initially considered for inert non-polar liquid. A molecule is formed when atoms combine to share one or more of their electrons. This rearrangement of electrons may cause an imbalance in charge distribution creating a permanent dipole moment. These moments are oriented in a random manner in the absence of an electric field so that no net polarization exists. In the presence of the field though, a torque is exercised on the electric dipole, which causes it to rotate and align itself with the electric field resulting in orientation polarization. If the field changes the direction, the torque will also change.

Interfacial or space charge polarization

Electronic, atomic, and orientational polarization occur when charges are locally bound in atoms, molecules, or structures of solids or liquids. Charge carriers also exist that can migrate over a distance through the material specifically visible when a low frequency electric field is applied. Interfacial or space charge polarization occurs when the motion of these migrating charges is impeded. The charges can be trapped within the interfaces of a material. Motion may also be hindered when charges cannot be freely discharged or replaced at the electrodes. Mixtures of materials with electrically conducting regions that are not in contact having barrier for charge carrier migration exhibit the Maxwell-Wagner effect at low frequencies. At these frequencies, the charges have time to accumulate at the

borders of the conducting regions causing ε' to increase. At high frequencies, polarization does not occur since the charge displacement is small compared to the dimensions of the conducting region and they do not have time to accumulate.

1.5 DC conductivity

The measured loss of material can actually be expressed as a function of both dielectric loss (ε_d'') and conductivity (σ_{dc}).

$$\varepsilon'' = \varepsilon_d'' + \frac{\sigma_{dc}}{\varepsilon_0} \quad (1.2)$$

At low frequencies, the overall conductivity can be made up of many different conduction mechanisms, but DC conductivity is the most prevalent in all materials. At low frequencies the effect of DC conductivity is inversely proportional to frequency and appears as a 1/f slope of the ε" curve with the ε' curve being a straight line. DC conductivity involves charge transport by particle hopping, with each ion having unrestricted access to a path connecting the electrodes.

1.6 Dielectric Permittivity

Spectroscopic dispersion of dielectric permittivity and associated energy absorption regions may be observed in a material over a range of 10^{11} to 10^{-6} Hz due to classical electrical polarization and conduction process. The magnitude of the effects and the frequency location of the energy absorption features associated with these processes will depend markedly upon the physical and chemical nature of the material and the temperature and pressure at which it is studied. The relaxation dynamics of soft matter, e.g. polymeric materials and glass-forming

liquids, is characterized by a large frequency range. It is based on the interaction of an external field with the electric dipole moment of the sample.

Dielectric spectroscopy has been recognized over the years and has an increasing influence as a tool for material characterization. It is beneficial in quality control, manufacturing and other applications of characterization in pharmaceuticals, biological systems, interfaces etc. Dielectric property shows relaxation or polarization of a dielectric. It is the ability of a material to polarize under the influence of an electromagnetic field. Technique to measure dielectric property of a material is dielectric spectroscopy as polarizability of a material depends on the structure and molecular properties. Dielectric spectroscopy is used as an investigative tool for the study of molecular motions of dipolar molecules in liquids and solids. It measures real and imaginary permittivity; over a wide frequency range (1 μHz- 1 THz) as a function of temperature. Assessments of interfacial polarization and conduction processes (low frequency) and dipole polarization effects (high frequency) can be done on the samples. The former can be related to the matrix-filler surface, while the latter gives information about the effect on the bulk material i.e. polymer. The technique is also used to study the hopping conduction of charged species in polar solids and semiconductors.

All dielectrics (except vacuum) have two types of losses. One is a conduction loss, representing the flow of actual charge through the dielectric, while the other is the dielectric loss due to rotation of dipoles in an alternating electric field. The conduction loss arises from the DC current which is due to the continuous motion of charges from one electrode to the other. The dielectric loss is characterized by

the polarization current which characterizes the adjustment of the polarizing species to a step function field. One way of describing the dielectric losses is to consider the permittivity as a complex number, defined as

$$\varepsilon * (\omega) = \varepsilon'(\omega) - i\varepsilon''(\omega) \quad (1.3)$$

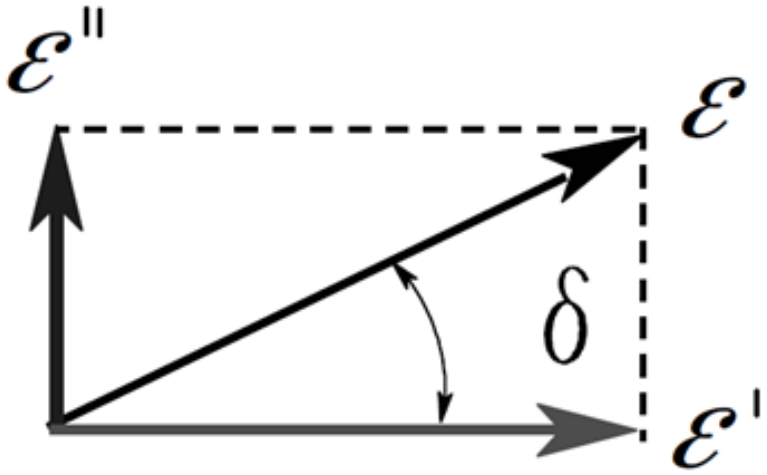

Figure 1.4: Complex permittivity diagram

The real part of permittivity (ε') is a measure of how much energy from an external electric field is stored in a material. The imaginary part of permittivity (ε") is called the loss factor and is a measure of how dissipative a material is to an external electric field. ε" is always greater than zero and is usually much smaller than ε'. The loss factor includes the effects of both dielectric loss and conductivity.

1.7 Structural Rearrangement and Relaxation

1.7.1 Debye and Non-Debye relaxation patterns.

All spectral relaxation functions can be described in terms of exponentially decaying elements and these functions need not be unique. Use of Debye- like relaxation element to describe experimentally observed response is just a mathematical transformation of the measured response unless the resulting distribution can be related to some other distributed property of the system. The physical origin of the Debye relaxation lies in the ensemble of non-interacting dipoles, each assigned a unique relaxation time due to its local environment. The environment remains unaffected by the relaxation processes (known as linear response) and the total relaxation is determined by summing (in parallel) the individual contributions. Debye model is completely restored if all dipoles relax identically. Another type of relaxation can occur in which the dipoles interact with their environment containing other dipoles building a finite-sized cluster. According to this phenomenon the relaxation proceeds in series as the slower components replace yet relaxed faster components. Therefore two physical categories can be described regarding relaxation i.e. ideal Debye case, ideal distribution having contributions in parallel from an ensemble, and the distribution having sequential developments in series for a range of interacting timescales. Presence of higher frequency relaxations for components of the same dipole extends the memory into timescale of relaxation giving rise to non-Debye behavior. As for the Debye case the knowledge of polarization at a single time is sufficient to describe the relaxation behavior for the entire timescale, which for a non-Debye behavior is not sufficient. A condition to describe to Debye relaxation

is to consider the rate of change of polarization to be proportional to the polarization hence

$$\frac{dP(t)}{dt} = -\frac{1}{\tau}P(t) \quad (1.4)$$

The time development of polarization is given by

$$\mathbf{P}(t) = \mathbf{P_0}(1 - e^{-\frac{t}{\tau}}) \quad (1.5)$$

And,

$$\mathbf{P}(t) = \mathbf{P_0}e^{-\frac{t}{\tau}} \quad (1.6)$$

for charge and discharge conditions respectively. Rate of change of polarization gives the current density flowing in an external circuit

$$\mathbf{j}(t) = \pm \mathbf{P_0}e^{-\frac{t}{\tau}}\boldsymbol{\tau}^{-1} \quad (1.7)$$

If the sample is polarized to an intermediate value of polarization $P_1 < P_0$ expressed as $P_0\exp(-t_d/\tau)$ and the discharge is delayed from time zero to time t_d then the current flowing in the external circuit is given by

$$j(t) = -P_0\exp(-t_d/\tau)\exp[-(t-t_d)/\tau]\tau^{-1} = -P_0\tau^{-1}e^{-t/\tau}\ ,\ t \geq t_d \quad (1.8)$$

Hence by the above formulation it can be defined that Debye relaxation can be described by the knowledge of initial polarization [2].

Usually, the measured dielectric spectrum is much “broader” than predicted by the Debye function. In a lot of cases the dielectric function is asymmetric signifying a short time (high frequency) behavior is more pronounced than the long time (low frequency) range. This behavior is called non-Debye or at times non-ideal dielectric relaxation behavior. Non-Debye behavior is based on the

assumption that the individual responses from the elemental sub-systems are in parallel. The external current is then represented for discharge conditions by

$$j(t) = -P_0 \int_0^\infty g(\tau)\tau^{-1} e^{-\frac{t}{\tau}} d\tau \qquad (1.9)$$

where g(τ) correlation factor is used to model the interaction between dipoles with respect to the ideal case of non-interacting dipoles. By assuming a polarization $P_d = P_0 \int_0^\infty g(\tau)\exp(-t_d/\tau)d\tau$, the discharge current is calculated when polarization P_d is delayed by time t_d given by

$$j(t) = P_0 \int_0^\infty g(\tau)\exp(-t_d/\tau)d\tau \int_0^\infty g(\tau)\tau^{-1}\exp[(-(t-t_d)/\tau)]d\tau \quad , t \geq t_d \qquad (1.10)$$

which can be equal to the current in Eq. (1.9) if g(τ) is δ-distribution (Dirac's distribution) in τ hence the case considered is recovered. If we consider two simultaneous Debye relaxation processes of equal strength and relaxation times τ_1 and τ_2 Eq. (1.10) becomes

$$j(t) = (P_0/4)\,[\tau_1^{-1} e^{-t/\tau_1}(1 + e^{t_d/\tau}) + \tau_2^{-1} e^{-t/\tau_2}(1 + e^{t_d/\tau})] \quad ,$$

$$t \geq t_d,\ \tau^{-1} = \tau_1^{-1} - \tau_2^{-1} \qquad (1.11)$$

This proves that relaxation current is strongly dependent on the parameters characterizing the distribution and the initial polarization is not sufficient to define the state of the system.

Maxwell's Equations describe the generation of magnetic and electric fields due to distribution and movement of electrically charged particles. Lorentz force law on the other hand describes the force acting on a point charge q in motion in the presence of electromagnetic fields further completing the Maxwell's

Equations. Lorentz force law is based on the effect of E and B, electric and magnetic fields respectively on a point charge. These point charges are all under the influence of other forces which Maxwell's equations denote by charge and current densities.

$$rot\, \boldsymbol{E} = -\frac{\partial}{\partial t}\boldsymbol{B} \quad (1.12)$$

$$rot\, \boldsymbol{H} = j + \frac{\partial}{\partial t}\boldsymbol{D} \quad (1.13)$$

$$div\, \boldsymbol{D} = \rho \quad (1.14)$$

$$div\, \boldsymbol{B} = 0 \quad (1.15)$$

Here **E** and **H** are the electric and magnetic fields respectively, **D** the dielectric displacement, **B** the magnetic induction, **j** the current density and $\boldsymbol{\rho_e}$ density of charges. If the electric field strength applied is low then **D** can be expressed as:

$$\mathbf{D} = \varepsilon^{*}\varepsilon_0\mathbf{E} \quad (1.16)$$

where ε_0 is the dielectric permittivity of vacuum and ε^{*} the complex dielectric function or dielectric permittivity. Maxwell's equations describe ε^{*} is time dependent if time dependent processes take place within the sample. Relaxation phenomena are related to molecular fluctuations in dipoles due to molecules. Drift motion of mobile charge carriers cause conductive contributions to the dielectric response. If a periodic electric field is applied as $\mathbf{E}(t) = \mathbf{E}_0\exp(-i\omega t)$ under the influence of time dependent processes and leading to a difference in the time dependencies of electric field and dielectric displacement. Complex dielectric function described by ε^{*} as:

$$\varepsilon^{*}(\omega) = \varepsilon'(\omega) - i\varepsilon''(\omega) \quad (1.17)$$

where $\varepsilon'(\omega)$ is the real part and $\varepsilon''(\omega)$ is the imaginary part of the complex dielectric function. Maxwell's equations proves the relation of complex dielectric function to the complex index of refraction by $\varepsilon^* = (n^*)^2$ ($n^*(\omega) = n'(\omega) + in''(\omega)$). Polarization **P** describes the dielectric displacement originated by the response of the sample to an external field. Hence:

$$\mathbf{P} = \mathbf{D} - \mathbf{D_0} = (\varepsilon^* - 1)\, \varepsilon_0\, \mathbf{E} = \chi^*\, \varepsilon_0 \mathbf{E} \qquad (1.18)$$

where $\chi^* = (\varepsilon^* - 1)$, χ^* is the dielectric susceptibility of the sample under the influence of an outer electric field. It provides a measure of how easily a dielectric material polarizes in the presence of an electric field. For high fields non-linear effects come into play and further complicate the mathematical formulation. Ohm's law provides the relation between electric field and current density with a coefficient known as the complex dielectric conductivity σ^* having time dependence according to $\sigma'(\omega) + i\sigma''(\omega)$. From the equations above we can conclude that the current density and the time derivative of the dielectric displacement are equivalent quantities. Therefore,

$$\mathbf{j} = \sigma^* \mathbf{E} \qquad (1.19)$$

$$\sigma^* = i\omega\, \varepsilon_0\, \varepsilon^* \qquad (1.20)$$

Considerable effects play a role, caused due to shielding of the outer electrical field. Shielding effects are due to a molecule with a permanent dipole surrounded by other particles, also known as local field effects. The field of the permanent dipole polarizes its environment proportional to its polarizability α. If the surrounding particles also contain permanent dipole moments their orientation is also influenced. First approach to the calculation of these two effects was done by

Lorentz. A cavity was considered in an infinitely extended media and polarization **P** was calculated. Assumption made was that the local electric field $\mathbf{E}_{loc}$ is proportional to the polarization of the cavity and the surrounding media can be described by static dielectric permittivity ε_s. For a sphere also called Lorentz sphere $\mathbf{E}_{loc}$ is described as:

$$\mathbf{E}_{loc} = \mathbf{E} + a_{lor}(\mathbf{P}/\varepsilon_0) \tag{1.21}$$

A macroscopic polarization is related to microscopic dipole moment $\boldsymbol{p_i}$ of particles with volume V by:

$$\mathbf{P} = \frac{1}{V}\sum p_i \tag{1.22}$$

Microscopic dipole moments have induced character due to a local electric field $\mathbf{E}_{loc}$ and vary linearly as $\mathbf{p} = \alpha\mathbf{E}_{loc}$ where α is the measure of the mobility of negative and positive charges. For apolar molecules the polarization induced by the outer electric field and Lorentz field is given by:

$$\mathbf{P} = \frac{N}{V}\alpha\boldsymbol{E} = \frac{N}{V}\frac{\varepsilon_s+2}{3}\boldsymbol{E} \tag{1.23}$$

For static case i.e. $\varepsilon_s = \lim_{\omega \to 0} \varepsilon'(\omega)$ hence Eq. (1.7) gives $\mathbf{P} = \varepsilon_0(\varepsilon_s - 1)\mathbf{E}$. Therefore we get:

$$\frac{\varepsilon_s-1}{\varepsilon_s+2}\frac{M}{\rho} = \frac{1}{3}\frac{N_A}{\varepsilon_0}\alpha \tag{1.24}$$

where N denotes the whole number of dipoles in the system, $\frac{N}{V}$ the volume density of dipoles also expressed as $\frac{\rho}{M}N_A$. M is the molar mass of the molecule, ρ the

density of the system and N_A the Avogadro number. As many molecules have permanent dipole moments μ which can be oriented by an electric field. Hence for a system containing one kind of dipoles we get from Eq. (1.23):

$$\mathbf{P} = \frac{1}{V}\sum \mu_i + \boldsymbol{P}_\infty = \frac{N}{V}\langle\mu\rangle + \boldsymbol{P}_\infty \qquad (1.25)$$

$\langle\mu\rangle$ is the mean dipole moment. For small interaction energies of a dipole with the electric field $\langle\mu\rangle$ is given as

$$\langle\mu\rangle = \frac{\mu^2}{3k_BT}\boldsymbol{E} \qquad (1.26)$$

Hence from the above equation **P** deduces to

$$\mathbf{P} = \frac{\mu^2}{3k_BT}\frac{N}{V}\boldsymbol{E} \qquad (1.27)$$

Therefore for polar molecules the contribution of orientational polarization to the dielectric function can be represented as

$$\varepsilon_s - \varepsilon_\infty = \frac{\mu^2}{3\varepsilon_0 k_BT}\frac{N}{V} \qquad (1.28)$$

The effect of orientation polarization on polar molecules is

$$\frac{\varepsilon_s-1}{\varepsilon_s+2}\frac{M}{\rho} = \frac{1}{3}\frac{N_A}{\varepsilon_0}\left(\alpha + \frac{\mu^2}{3k_BT}\right) \qquad (1.29)$$

also known as the Debye-formula [3].

In dielectrics perturbation is described by the time dependent external electric field x(t) = E(t) and the response of the system is polarization y(t) = P(t). Hence by linear response theory we deduce

$$\mathbf{P}(t) = \mathbf{P}_\infty + \varepsilon_0\int_{-\infty}^{t}\varepsilon(t-t')\frac{dE(t')}{dt'}dt' \qquad (1.30)$$

ε(t) represents the time dependent dielectric polarization and P_∞ ranges over all contributions from induced polarization. If a periodic perturbation $\mathbf{E}(t,\omega) = \mathbf{E}_0\exp(-i\omega t)$ is applied with angular frequency ω, Eq. (1.30) reduces to

$$\mathbf{P}(\omega) = \varepsilon_0 (\varepsilon^*(\omega) - 1)\, \mathbf{E}(\omega) \quad (1.31)$$

ε*(ω) is a complex dielectric function of the form ε'(ω) – iε"(ω) where ε'(ω) is proportional to the energy stored reversibly in the system per period and ε"(ω) is proportional to the energy dissipated per period. Therefore the relationship of ε*(ω) with the time dependent dielectric function is given by

$$\varepsilon^*(\omega) = \varepsilon'(\omega) - i\varepsilon''(\omega) = \varepsilon_\infty - \int_0^\infty \frac{d\varepsilon(t)}{dt} \exp(-i\omega t)\, dt \quad (1.32)$$

One of the simplest assumptions post negligence of inertia effects to calculate the time dependence of dielectric behavior is change of polarization is proportional to its actual value

$$\frac{dP(t)}{dt} = -\frac{1}{\tau_D} \boldsymbol{P}(t) \quad (1.33)$$

where τ_D is the characteristic relaxation time. This leads to an exponential decay for the correlation function $\boldsymbol{\phi}(\tau)$ giving

$$\boldsymbol{\phi}(\tau) = \exp\left[-\frac{t}{\tau_D}\right] \quad (1.34)$$

$\boldsymbol{\phi}(\tau)$ represents the correlation function of the polarization function. The complex dielectric function obtained henceforth is

$$\varepsilon^*(\omega) = \varepsilon_\infty + \frac{\Delta\varepsilon}{1 + i\omega\tau_D} \quad (1.35)$$

1.7.2 Primary or α-Relaxation

Structural disordered nature of glass-forming melts gives rise to non-Arrhenius and non-exponential behavior of their dynamics. There are many experimental techniques that are applied to understand responses related to primary structural relaxations. Study of spatial heterogeneity provides the step to understand the

relation between macroscopic properties of soft condensed matter and its molecular mechanisms. Mechanical shear stress measurements, nuclear magnetic resonance techniques, dielectric relaxation, various light scattering and photon correlation spectroscopies, enthalpy or volume recovery after a temperature jump, dynamic heat capacity and thermal expansivity methods and neutron scattering are some of the techniques applied to study responses. To study the responses a perturbation is applied at time zero and a gradual approach towards equilibrium as function of time is measured. For very small perturbations the shape is studied solely by the equilibrium fluctuations as stated by the fluctuation-dissipation theorem (FDT).

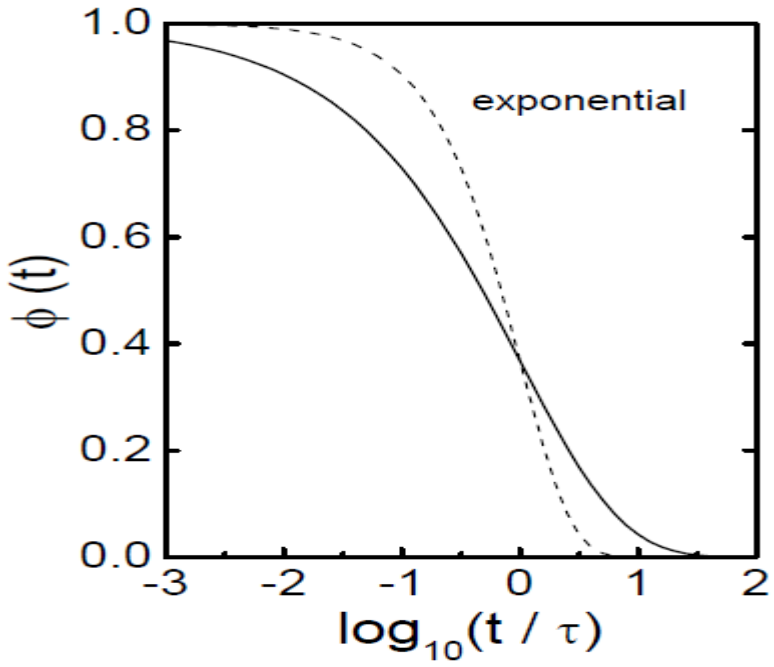

Figure 1.5: Solid line shows the correlation function for the non-exponential feature while dashed line shows for the exponential feature.

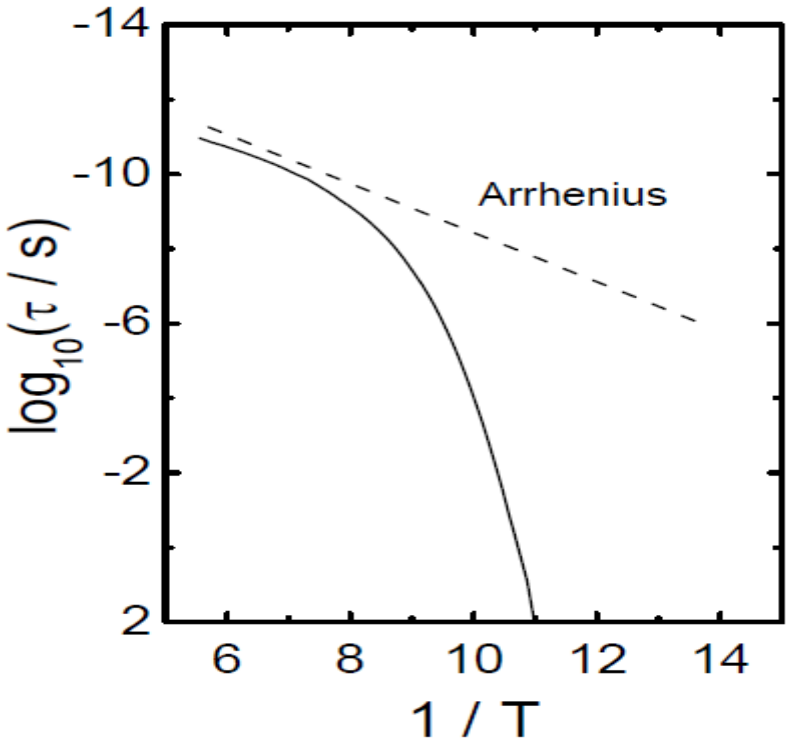

Figure 1.6: Dashed line shows Arrhenius feature and solid line non-Arrhenius feature for activation scheme of different materials.

The non-exponential relaxations in disordered materials as shown above by the solid line follows the stretched exponential or Kohlrausch-Williams-Watts (KWW) type decay

$$\Phi(t) = \phi_0 \exp\left[-\frac{t}{\tau_{KWW}}\right]^{\beta_{KWW}} \qquad (1.36)$$

β_{KWW} is the term used to describe the degree of relaxation time dispersion. Small β_{KWW} means more dispersive relaxation and it decreases if temperature goes below T_g. For the Debye case $\beta_{KWW} = 1$ and for general purposes it is considered to be $\beta_{KWW} = 0.5$.

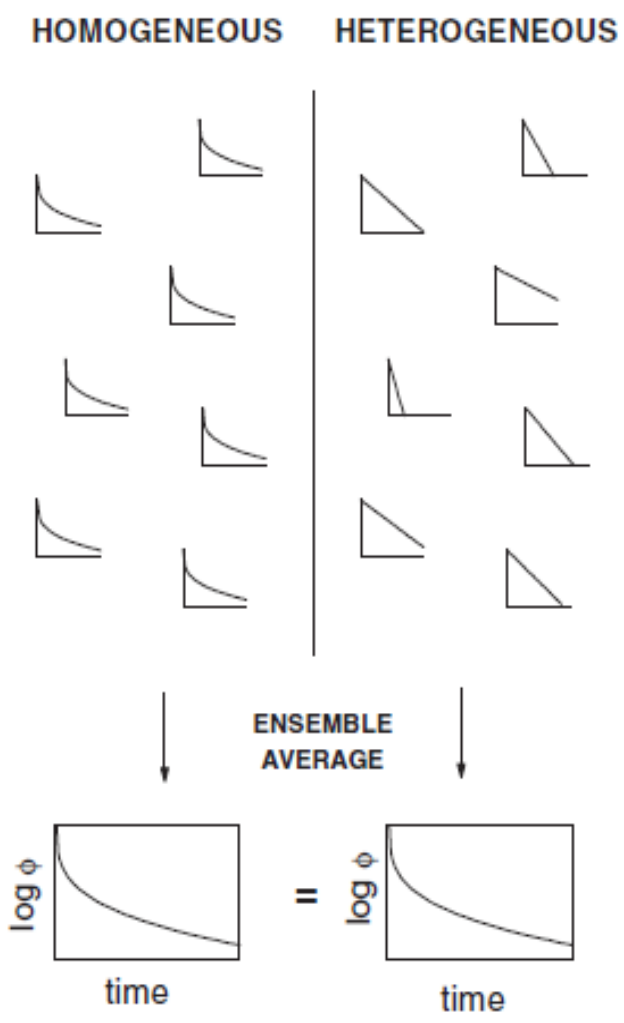

Figure 1.7: Schematic representation of two different sources of non-exponential correlation decays [4].

The correlation function can be expressed as a superposition of exponentials for the relaxation time τ

$$\Phi(t) = \int_0^\infty g(\tau)\, e^{-\frac{t}{\tau}} d\tau = \langle \exp\,(-t/\tau) \rangle \qquad (1.37)$$

As shown in the figure above in the spatially homogeneous case the sample contributes identically to the relaxation function having local and ensemble averaged dynamics as same. On the other hand for the heterogeneous case each

local relaxation is associated with pure exponential dynamics with spatial contribution of time constants imbibed to arrive at non-exponentiality of the ensemble average. When a material is cooled to near its melting temperature T_m the discontinuous changes of the material properties remain absent. In a narrow range near T_m, viscosity η and τ increase by 12 orders of magnitude while in the equilibrium liquid state. Average relaxation times of glass-forming liquids are characterized by a deviation from Arrhenius behavior but liquids above T_m show the dynamics closer to the Arrhenius behavior. The temperature dependence of glass-forming liquids is explained by Vogel-Fulcher-Tammann (VFT) law

$$\tau(T)=\tau_0 \exp\left[\frac{DT_0}{T-T_0}\right] \quad (1.38)$$

used to characterize the temperature dependence of transport coefficients in the regime of the equilibrium liquid. An alternative approach to arrive at a VFT type τ(T) was made by Adam and Gibbs in terms of 'cooperatively rearranging regions' (CRRs) having a link between the temperature-dependent configurational entropy $S_c(T)$ and the relaxation time

$$\tau(T) = \tau_0 \exp\left[\frac{c}{TS_c(T)}\right] \quad (1.39)$$

where $S_c(T) = S_\infty - K/T$. Several other approaches were taken to explain the single VFT curve with temperature dependence as

$$\log_{10}(\tau/s)=A+B/(T-T_0) \quad (1.40)$$

where A and B signify terms (expressions) equivalent to Eq. (1.38) respectively.

1.7.3 Secondary or β-relaxation Process

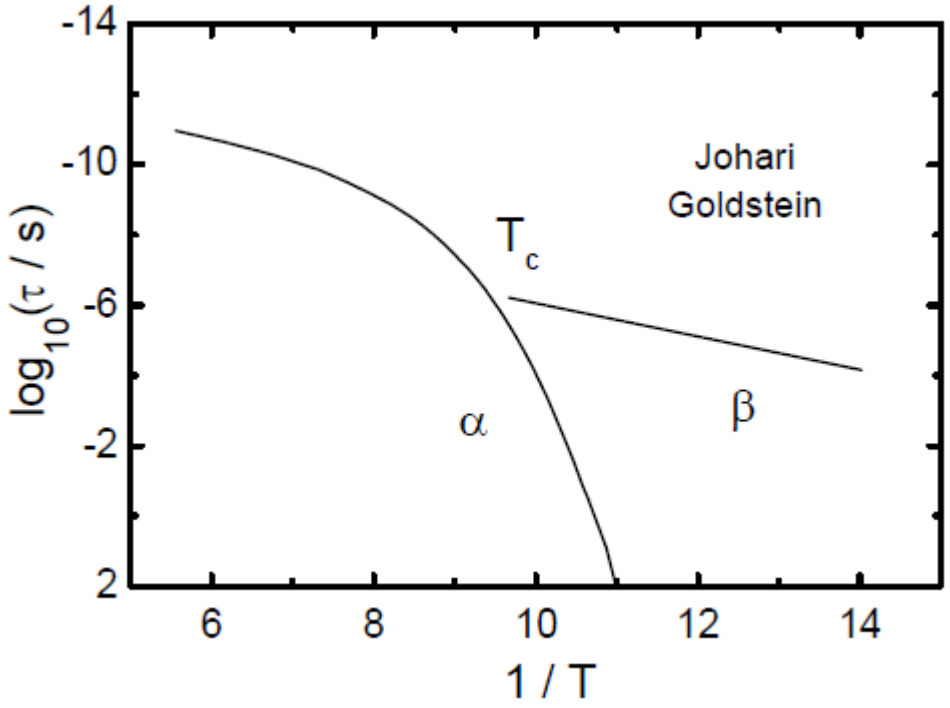

Figure 1.8: Schematic representation of α and β relaxations in supercooled liquids. As shown above the β relaxation displays Arrhenius temperature dependence and merges with α-relaxation (primary relaxation process at in liquid state) near a crossover temperature T_C. α-relaxation signifies cooperative rearrangements related to structure which determine glass transition. The secondary or smaller process known as the β-relaxation part from the α-relaxation also occurs near glass transition. It also termed as β_{slow} or Johari-Goldstein (JG) β relaxation. It signifies the faster and more localized motion of the molecules and is highly material dependent not distinct for all the glass-formers. B-relaxation has three dynamic types: i) Arrhenius temperature dependence that merges with α-relaxation at the crossover temperature T_C. ii) Symmetric Cole-Cole type dispersion of relaxation. iii) Increase of dielectric strength with temperature.

As per the above discussion all disordered systems exhibit dispersion in relaxation times often observed as a non-exponential correlation function described by KWW. Other non-exponential functions which are empirical fit functions used to describe the dispersion are Cole-Cole (γ =1), Cole-Davidson (α=1) and Havriliak-Negami ($0<\alpha$, $\alpha\gamma \leq 1$) as

$$\varepsilon^*(\omega) = \varepsilon_\infty + \frac{\varepsilon_s - \varepsilon_\infty}{[1+(i\omega\tau)^\alpha]^\gamma} \quad (1.41)$$

The deviations from simple behavior i.e. non-Arrhenius and non-exponential character in liquid dynamics vary systematically along the strong fragile pattern of glass-forming materials. Fragility m characterizes how rapidly the dynamics of a material slows down as it is cooled toward the glass transition temperature. High-fragility represents narrow glass transition temperature region vis-à-vis low-fragility shows broad glass transition when normalized to T_g. It is represented by the slope of the viscosity of a material with temperature as it approaches glass transition

$$m=\left(\frac{\partial log_{10}\eta}{\partial(T_g/T)}\right)_{T=T_g} \quad (1.42)$$

1.8 Energy stored in a Capacitor

When a potential difference $V(t) = V_0 \cos\omega t$, (V_0 is the absolute value of voltage applied) is applied to an empty parallel plate capacitor it will cause a current $i(t) = -\omega C_0 V \sin\omega t$ to flow to the plate. The capacitance of a capacitor can be expressed as

$$C_0 = A\sigma/V \quad (1.43)$$

where A is the area of the capacitor, σ the charge density and V the potential difference across the plates. The power supplied to the capacitor is

$$w(t) = i(t)V(t) = -\omega C_0 V_0^2 \sin\omega t\cos\omega t = -\frac{1}{2}\omega C_0 V_0^2 \sin 2\omega t \quad (1.44)$$

As we can see above the power supplied varies at twice the frequency of the applied potential difference. The negative sign arises as Vt decreases after t=0. Power leaves the capacitor in the first quarter period where $0<t<T/4 = \pi/2\omega$ while in the next quarter period power is transferred from the generator to the capacitor. Hence the maximum energy stored in the capacitor is

$$U_{max} = \frac{1}{2}\omega C_0 V_0^2 \int_0^{\frac{T}{4}} dt \sin 2\omega t = \frac{1}{2} C_0 V_0^2 \quad (1.45)$$

The presence of a dielectric changes the magnitude and phase of the current therefore it can be represented as

$$i(t) = \omega C_0 V_0 \cos(\omega t + \pi 2)$$

$$= \mathrm{Re}(\omega C_0 V_0 \exp[i(\omega t + \pi/2]) = \mathrm{Re}(i\omega C_0 V_0 \exp(i\omega t)) \quad (1.46)$$

And as the dielectric is present absolute value of current can be expressed as

$$I_0 = i\omega C(\omega) V_0 \quad (1.47)$$

Experimentally it has been found that

$$C(\omega) = \varepsilon(\omega)\, C_0 \quad (1.48)$$

where $\varepsilon(\omega) = \varepsilon'(\omega) - i\varepsilon''(\omega)$ is the complex relative permittivity.

As shown, I_0 has two components, one that is in quadrature with V_0 leading it by $\pi/2$

$$I_{0q} = i\omega\varepsilon'(\omega) C_0 V_0 \quad (1.49)$$

And the other is in parallel to V_0 which is in phase with it

$I_{oi} = \omega\varepsilon''(\omega)C_0V_0$ (1.50)

I_{0q} arises from the reversible charging and discharging of the capacitor while I_{0i} represents the dissipation of electrical energy into heat which is not accounted for by the former component. Therefore the maximum energy stored in the capacitor is

$U_{max} = \frac{1}{2}\varepsilon' C_0 V_0^2$ (1.51)

The one cycle average of w is defined by w^T by

$w^T = \frac{1}{T}\int_0^T dtw(t)$ (1.52)

Hence we can find one cycle average by

$w(t)^T = \frac{1}{2}\omega\varepsilon''(\omega)C_0V_0^2 = \frac{1}{2}\frac{\varepsilon''}{|\varepsilon|}|I_0||V_0|$ (1.53)

The phase angle ϕ i.e. the angle by which the current leads the voltage is determined by

$\tan\phi = (|I_{0q}|/|I_{0i}|) = \frac{\varepsilon'(\omega)}{\varepsilon''(\omega)}$ (1.54)

where $\sin\phi = \varepsilon'(\omega)/|\varepsilon(\omega)|$ and $\cos\phi = \varepsilon''(\omega)/|\varepsilon(\omega)|$ and $|\varepsilon(\omega)| = \{[\varepsilon'(\omega)]^2 + [\varepsilon''(\omega)]^2\}^{1/2}$.

Therefore Eq. (1.53) becomes

$w(t)^T = \cos\phi \left(\frac{|I_0|}{\sqrt{2}}\right)\left(\frac{|V_0|}{\sqrt{2}}\right) = \cos\phi I_{rms}V_{rms}$ (1.55)

cosϕ is known as the loss factor and signifies the in-phase behavior of current and voltage when ϕ = 0, on the other hand if ϕ=π/2 current and voltage are in quadrature and no dissipation of electrical energy into heat takes place. Materials that have low values of cosϕ are said to be low-loss and have great technical

importance. It is also expressed in terms of a complementary angle $\delta = \pi/2 - \phi$. As $\cos\phi = \sin\delta$ then it is safe to assume for small values of δ that

$$\cos\phi \approx \tan\delta \tag{1.56}$$

Hence for low loss materials we derive from Eq. (1.55),

$$\tan\delta \cong \frac{w(t)'}{I_m V_m} = \cot\phi = \frac{\varepsilon''(\omega)}{\varepsilon'(\omega)} \tag{1.57}$$

It is generally recognized that dielectric relaxation experiments involve a power density p with which energy is transferred irreversibly to the sample. According to Joule's law [5], the power density p absorbed is the field **E** times the in-phase component of σ'**E** of the current density **j**

$$\mathbf{p} \propto \sigma'|\mathbf{E}|^2 = \omega\varepsilon_0\varepsilon''|\mathbf{E}|^2 = \omega\varepsilon_0\varepsilon'\tan\delta|\mathbf{E}|^2 = \frac{1}{2}\omega\varepsilon_0\varepsilon''E_0^2 \tag{1.58}$$

where σ' is the real part of conductivity $\sigma^*(\omega)$.

Chapter 2

DESIGN AND MODELS

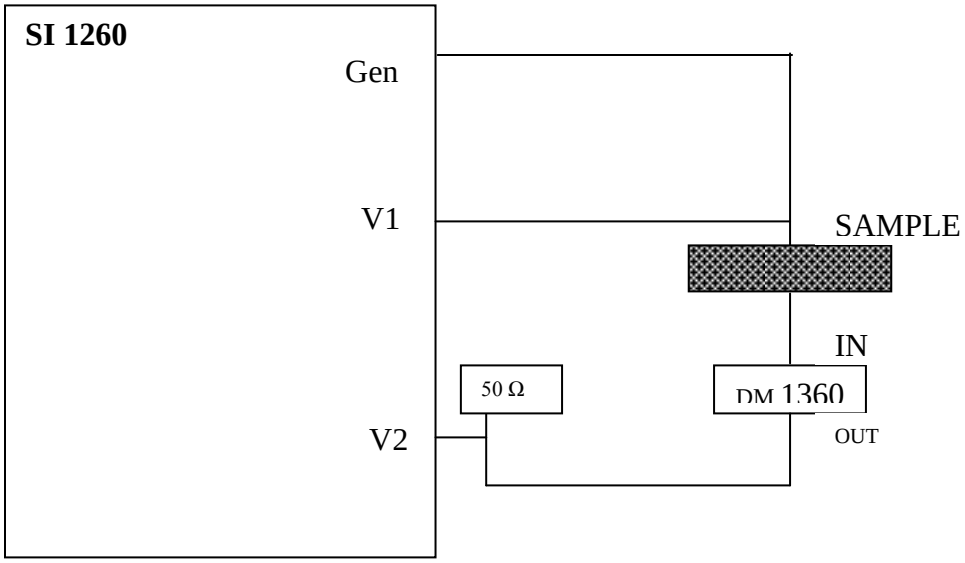

Figure 2.1: Schematic representation of low field dielectric measurement using a Solartron SI1260 gain phase analyzer and Leybold RDK 6-320/Coolpak6200 closed-cycle helium refrigerator with Lakeshore Mod. 340 controller equipped with calibrated DT-470-CU diode sensors.

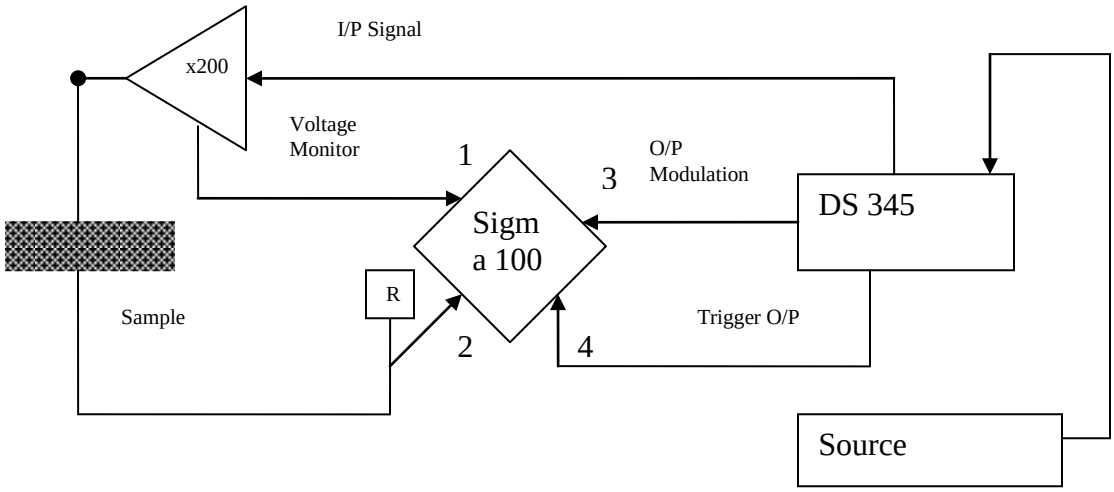

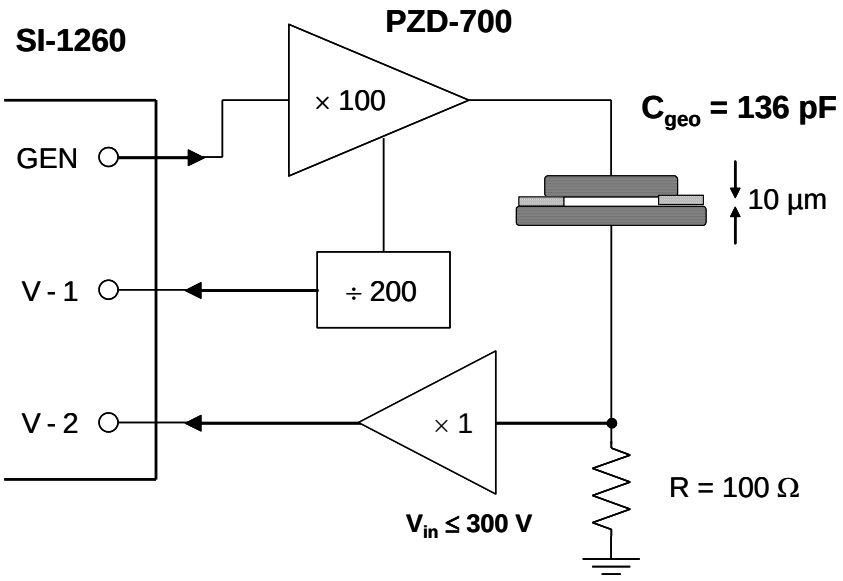

Fig. 2.2: Schematic representation of time –resolved measurement of a dielectric sample using a Trek PZD-700 high-voltage amplifier. The cryostat used for temperature control of the sample cell is Leybold RDK 6-320/Coolpak6200 closed-cycle helium refrigerator with Lakeshore Mod. 340controller equipped with calibrated DT-470-CU diode sensors. The applied voltage is originated from a programmable function generator (SRS DS-345) and a digitizing oscilloscope (Nicolet Sigma 100) records voltage across and current through the sample (using a shunt of order R = 1kΩ).

The impedance for frequencies between 1Hz and 50kHz is measured by a Solartron SI-1260 gain/phase analyzer, with the generator voltage amplified using a Trek PZD-700 high-voltage amplifier. The voltage at the sample is recorded via input V1 of the SI-1260 using the voltage monitor output of the amplifier, the current is recorded via input V2 as the voltage drop across a 100 Ω resistor. A voltage follower protects the SI-1260 V2 input against high voltages in case of a

sample failure. This circuit is based upon the AD-549L operational amplifier [6], and protects against 300V. The finite bandwidths of both the high voltage and the buffer amplifiers are found by reference measurements with virtually loss free capacitors. Sinusoidal electric fields, $E(t) = E_0 \sin\omega t$, with zero dc offset are applied to the sample. The SI-1260 is programmed to apply the high voltage for about 30 ms, with only the final 20 ms being used for data acquisition and analysis in order to suppress transient effects.

For the time-resolved measurements, liquid samples are prepared between two-polished stainless steel electrodes (16mm and 20mm diameter), separated by a Teflon ring of 10μm thickness with 14mm inner and 20mm outer diameter that covers the electrode edge. One electrode is spring loaded to maintain a temperature invariant stress on the Teflon ring. The cryostat used for temperature control of the sample cell is Leybold RDK 6-320/Coolpak6200 closed-cycle helium refrigerator with Lakeshore Mod. 340 controller equipped with calibrated DT-470-CU diode sensors. The applied voltage originated from a programmable function generator (SRS DS-345) and a digitizing oscilloscope (Nicolet Sigma 100) records voltage across and current through the sample (using a shunt of order $R = 1k\Omega$). Repetition rates of order $r = 0.1$ Hz are used, implying that the high field duty cycle remains small (≤ 0.1) and the sample is given ample time to equilibrate between energy absorption intervals. The oscilloscope can average over up to 5000 repeated signals so that a resolution of up to 5×10^{-5} regarding $\tan\delta$ for a particular period is achieved. The goal of this technique is to change the

field amplitude from one period to the next and monitor the changes with a period-by-period time resolution as shown below

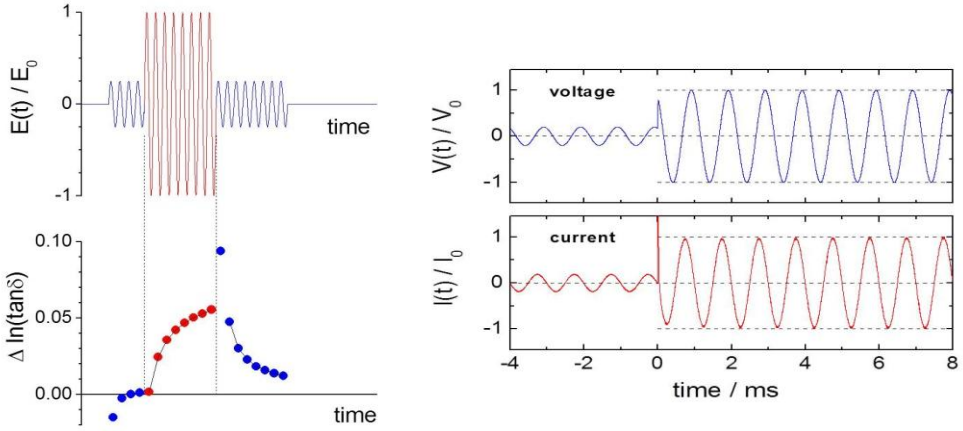

Figure 2.3: Setup for time-resolved impedance measurement based on the SRS DS-345 generator and Nicolet Sigma 100 oscilloscope. High voltages are provided by a Trek PZD-700 amplifier with built in voltage monitor signal for a direct return to the CH-1 input. The current is measured at the Ch-2 input as voltage as voltage drop across a resistor. The graph on the left indicates a arbitrary waveform signal and a typical response in terms of the relative change in tanδ. The graph on the right reflects amplitude modulation signal signifying an out of phase increase in cycles when high field is applied.

Various modes of the function generator are employed that exploits the arbitrary waveform (16300 points, 12 bit) and arbitrary modulation (10000 points, 16 bit) features. Programmed waveforms used are of the form $A(t)=A_0\ [(1-a)\sin(\omega t)+a\sin(n\omega t)$ where a = 0.2 which is a typical value for the relative amplitude of the higher harmonic and $1 \leq n \leq 16$ is a positive integer indicating frequency ratio of the two components. The waveform can have 32 periods, with A_0 = 0.2 for the first few periods, A_0 =1 for the following periods and again returning to A_0 =0.2

for the remainder of the periods. Each fundamental period is defined by 16000/(number of periods) = number of points in time i.e. 16000/32 = 500 points in time for the case above. The increase and decrease in the amplitude facilitates measuring the dielectric behavior in terms of tanδ followed by the addition or removal of power absorbed from the field. A change in the amplitude by a factor changes the power absorbed by the square of the amplitude. The amount of fundamental periods within the waveform is limited by requiring that each period uses at least 250 points limiting to $N \leq 64/n$. There are three modes used which are: i) As shown above the waveform is generated at a given repetition rate r. For intermediate times, the voltage remains at zero. The limitation of this method is regarding the number of periods, but the advantage is that the amplitude change is in phase with the sine waves. ii) The amplitude factor A_0 remains constant throughout the waveform with a sequence of m waveforms generated in burst mode at a given repetition rate r. Intermediate amplitudes cannot be attained in this mode due to absence of signal before or after the high voltage but it provides large number of periods at high resolution. Low field data is recorded separately. iii) The waveform is subjected to an arbitrary amplitude function with a continuous output applied at a given repetition rate. Large number of periods is attainable combined with a transition from low to high voltage, but amplitude transition does not coincide with the beginning of a period.

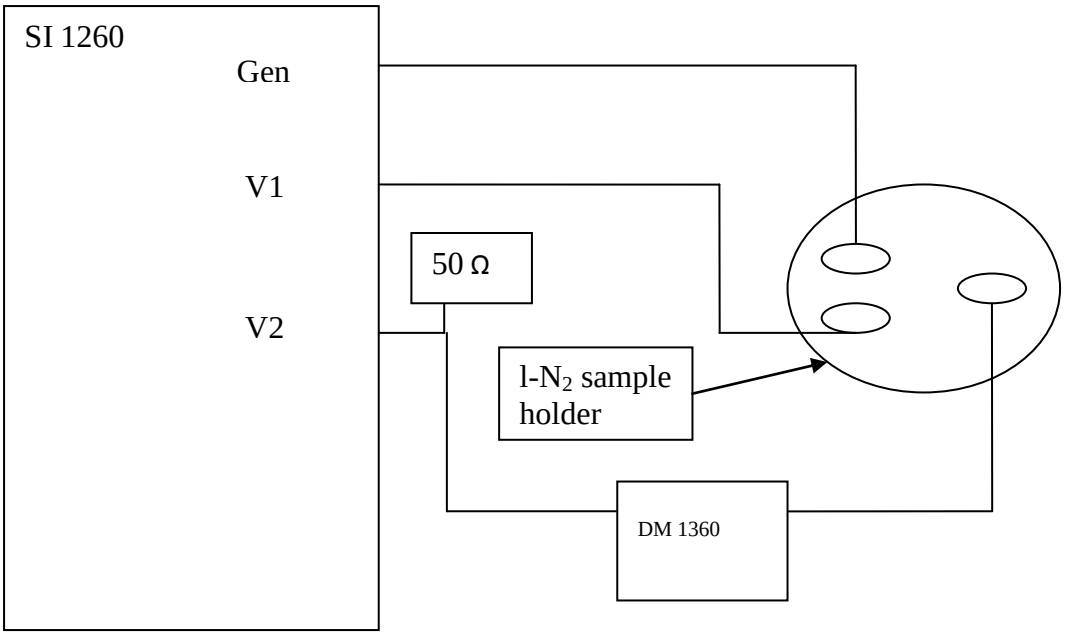

Fig 2.4: Schematic representation of low field dielectric measurement using a Solartron SI1260 gain phase analyzer and a Novocontrol l-N_2 cryostat with Quatro controller.

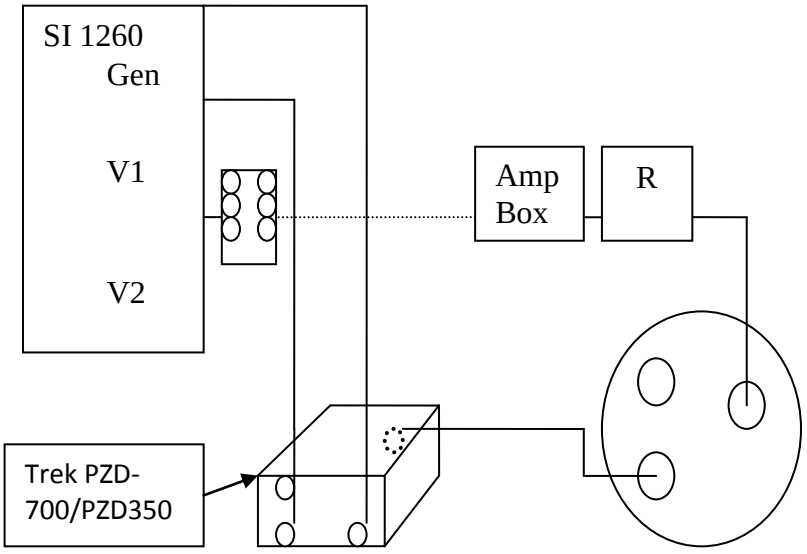

Fig. 2.5: Schematic representation of high-field dielectric measurement using a Solartron SI1260 gain phase analyzer and AD-549L/OP654L operational amplifier with a Trek PZD-700/PZD350 high-voltage amplifier. The cryostat used is Novocontrol l-N_2 cryostat with Quatro controller.

The technique facilitates changing the field amplitude from one period to the next and to monitor the changes with a period-by-period time resolution. The amplitude change by a factor of 5 is under control of an arbitrary amplitude function that is cycled at the given repetition rate. In this manner, the transition from low to high voltage and back can be programmed without limitation on the number of cycles associated with high fields, but the amplitude transition does not necessarily coincide with the beginning of a period.

The two signals, voltage V(t) and current I(t), are subject to period-by-period Fourier analysis according to

$$R = \frac{\omega}{\pi}\int_0^{2\pi/\omega} \sin(\omega t) S(t) dt = A\cos(\varphi)$$
$$I = \frac{\omega}{\pi}\int_0^{2\pi/\omega} \cos(\omega t) S(t) dt = A\sin(\varphi) \qquad (2.1)$$

where S(t) = V(t) or I(t) for analyzing voltage or current respectively. The amplitude is obtained by A = $\sqrt{R^2 + I^2}$ and the phase by φ = arctan (I/R). For each of the 1000 to 4000 periods measured in one frame, defining V_0, φ_V, I_0 , and φ_I with respect to the notation $V(t) = V_0\sin(\omega t + \varphi_V)$ and $I(t) = I_0\sin(\omega t + \varphi_I)$. The loss tangent, tanδ turns out to be the most robust quantity for measuring how energy absorption modifies the dynamics of the system, and its value is determined using $\tan\delta = \tan(\pi/2 - \varphi_V + \varphi_I)$. These techniques facilitate

monitoring the time-evolution of the field induced changes after applying or removing the high electric field. Although the system is generally not in equilibrium during these measurements, we continue to use notations such as tanδ, ε', and ε" that are actually meant to reflect equilibrium situations. The code performing the Fourier analysis also evaluates the power transferred irreversibly to the sample,

$$P=\overline{VI} = \frac{1}{2}V_0 I_0 \cos(\varphi_I - \varphi_V) = \frac{1}{T}\int_t^{1+T} V(t)I(t)\,dt \qquad (2.2)$$

We chose the VI-integration approach because this is correct also in the case of deviations from pure harmonic signals. Additionally, the permittivity and loss are computed via

$$\varepsilon'(\omega) = \frac{I_0 \sin(\varphi_I - \varphi_V)}{V_0 \omega C_{geo}}$$

$$\varepsilon''(\omega) = \frac{I_0 \cos(\varphi_I - \varphi_V)}{V_0 \omega C_{geo}} \qquad (2.3)$$

so that consistency with standard impedance results, $\varepsilon^*(\omega) = \varepsilon'(\omega) - i\varepsilon''(\omega)$, can be verified. Here $C_{geo} = \varepsilon_0 A/d$ is the geometric capacitance.

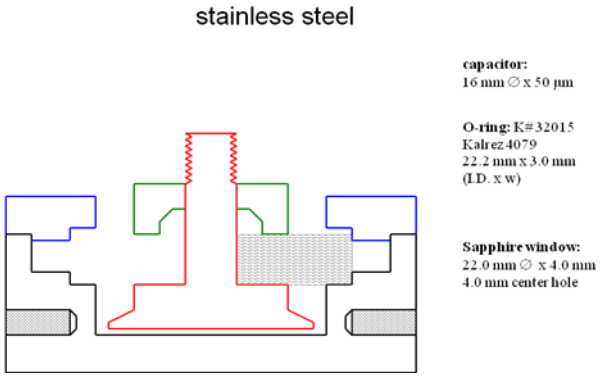

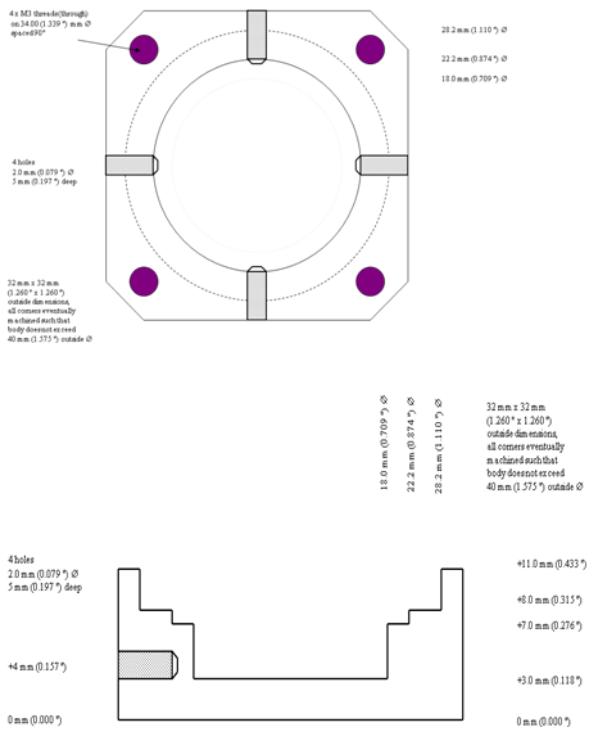

Figure 2.6: Schematic diagram of stainless steel dielectric steel with polished metal surfaces.

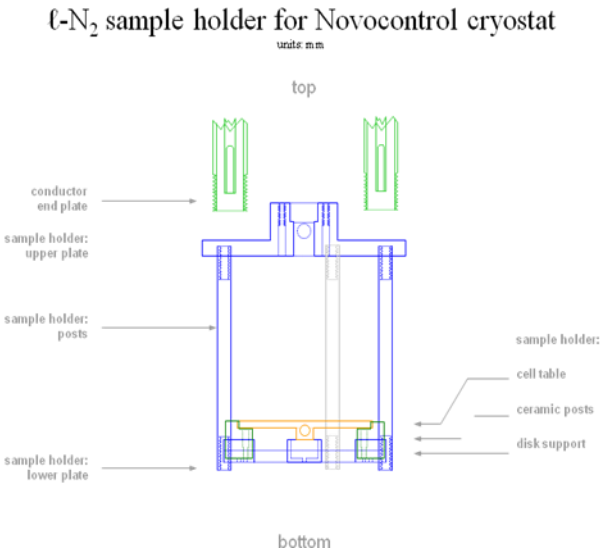

Figure 2.7: Schematic diagram of the l-N_2 sample holder for Novocontrol cryostat.

Chapter 3

THEORY

The behavior of glass-forming liquids is studied by relaxation experiments as dielectric spectroscopy or dynamic mechanical analysis. When an external field is applied within the regime of linear response, fluctuation dissipation theorem relates it to the equilibrium fluctuation of the system [7]. Disordered structure of liquids is studied by non-exponential function which restores the equilibrium. Heterogeneous dynamics in such systems leads to dynamically distinct domains having spatially varying relaxation times. The experiments are performed in the viscous state near the glass transition temperature T_g having pronounced relaxation time dispersions. Sample displaying relaxation modes absorbs energy by the slower degrees of freedom. Dielectric hole-burning method is used to study the dynamic heterogeneity for the reorientational motion of molecules and polymer segments [8-10]. It is a non linear method to study spectral selectivity exploiting the effects of energy absorbed from large external time-dependent fields. It is used to rationalize the nonlinear dielectric effects. The energy absorbed is translated to increase the fictive temperature T_f through the frequency dependent heat capacity. The fictive temperature plays a role in decreasing the relaxation time τ according to apparent activation energy $\partial \ln\tau/\partial(1/T)$. As shown below we can see the frequency dependence of ε" and ε' which depends on dielectric and thermal relaxation. As known, heat transport is governed by the value of heat conductivity κ that reflects the dispersive thermal relaxation times and excess fictive temperatures. Slower degrees of freedom are associated with

values of κ much below the phonon counterpart [11]. Model calculations are carried out for heterogeneous dynamics by considering the liquid consisting of dynamically distinct domains within which dielectric and thermal relaxation proceed exponentially with a distinct time constant. As the figure reflects the variation in the modes is due to the assumption of interaction among dynamically distinct domains. The frequency dependent dielectric function $\varepsilon^*(\omega) = \varepsilon'(\omega) - i\varepsilon''(\omega)$ is expressed as a superposition of Debye processes as

$$\varepsilon^*(\omega) = \varepsilon_\infty + (\varepsilon_s - \varepsilon_\infty)\int_0^\infty g(\tau)\frac{1}{1+i\omega\tau}d\tau \qquad (3.1)$$

where $g(\tau)$ represents the relative number of relaxing units associated with dielectric time constants between $\tau + d\tau$. For glycerol it has been shown that $g(\tau)$ is identical for dielectric relaxation $\varepsilon^*(\omega)$ and for dynamic heat capacity $c_p^*(\omega)$[12].

Dielectric relaxation experiments performed at dielectric fields that take the sample beyond the regime of linear responses provide information which is not available from low field counterparts [13-16]. In dielectric saturation polarization magnitude remains below the linear field dependence because the dipole orientation has an upper limit given by $\langle\cos\theta\rangle \leq 1$. Nonlinear effects stem from the energy a sample can absorb from an external field at high fields [17-18]. It is generalized that dielectric relaxation experiments involve a power density p with which energy is transferred irreversibly to the sample. An assumption considered is that the amount of energy involved is marginal and insufficient for modifying the dielectric behavior of the sample. External electric fields are

exploited to heat chemicals or food as in a microwave oven [19] which drives the sample beyond its linear regime. The sample properties remain unchanged and polarization is proportional to the field amplitude. The idea that irreversible energy transfer will modify the mode that absorbed it has been in non-resonant hole-burning experiments to study the heterogeneous aspect of dynamics that is particularly pronounced for glass-forming liquids in their viscous regime. Such supercooled liquids are known to display a distribution of relaxation times in their linear susceptibilities [20]. If these faster and slower modes are relaxing independently then energy absorbed selectively in a certain spectral region will not have the same effect as an increase in the macroscopic real temperature. Dielectric hole-burning has demonstrated that the non-exponential character of the overall relaxation originates from a superposition of exponential modes which relax highly independently regarding both polarization and enthalpy content. Non-linear impedance techniques have also been employed to study the conductivity at high fields. A recent application of dielectric relaxation experiments in the non-linear regime is that it links the non-linear susceptibility to the number of particles that are dynamically correlated [21-22]. When a dielectric is exposed to time dependent field, the system is not in equilibrium and the bath temperature is no longer sufficient for defining the state and behavior of the material.

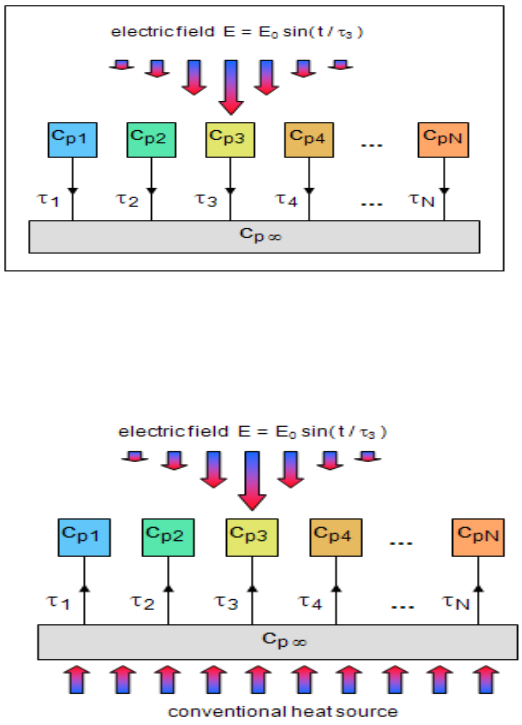

Figure 3.1 Schematic representation of heat capacities in a supercooled liquid with heterogeneous dynamics. About half of the total C_p is in fast modes ($C_{p\infty}$) while the remainder is associated with slow modes ($C_{p1....}$ C_{pN}) subject to a dispersion of relaxation times (τ_{1} $_{....}\tau_{N}$). The graph emphasizes the difference in the direction of heat flow and spectral selectivity for conventioanl heating (right) and heating via a time dependent field (left)[23].

In order to appreciate the difference between standard heating and the effect of energy absorption from a field, one has to realize that a time dependent field affects the dipolar degrees of freedom of a dielectric, and only eventually is this energy converted to heat and measurable as a temperature increase. The energy absorbed by a dielectric can modify the dynamics of the system via

different effects: either by elevating the fictive temperatures (configurational temperatures, dipole temperatures) of the modes that are involved in the absorption process, or by a change in the real measurable temperature, or both. Non-linear dielectric experiments such as the hole-burning approach focus on the changes of the fictive temperature, and these experiments are designed to maintain isothermal conditions. In the case of microwave chemistry or the use of a household type microwave oven, it is obviously the elevation of the real temperature that is targeted.

Dielectric relaxation is used to study relaxation patterns of supercooled liquids. For majority of liquids, the calorimetric glass transition temperature $T_{g\text{-}cal}$ is determined by the onset temperature of the heat capacity jump from the glassy to the liquid state. It is comparable to the kinetic glass transition temperature $T_{g\text{-}kin}$ where the average structural relaxation time approaches 100 seconds. For monohydroxy alcohols and some hydrogen bonding liquids the correlation is more complicated as the dielectric spectra has one pronounced Debye type (exponential) dielectric relaxation process and a smaller and faster non-Debye process. This is in contrast to the general spectra of generic glass-formers exhibiting one primary or α-relaxation which is non-exponential (non-Debye) in the supercooled regime. In the case of monohydroxy alcohols these are known as 'Debye-type' liquids and these two dielectric relaxation patterns give the Debye peak and the non-Debye α-relaxation. When heat capacity measurements are performed on these alcohols they do not exhibit two transitions [24]. Basic observations for Debye relaxations have shown that this peak is inconsistent with

the characteristics of structural relaxations. The exponential behavior contrasts the correlation linking the broadening parameter of relaxation times to the liquid fragility based upon numerous non-Debye supercooled liquid dynamics [25].

Chapter 4

RESULTS AND DISCUSSION

4.1 Glycerol

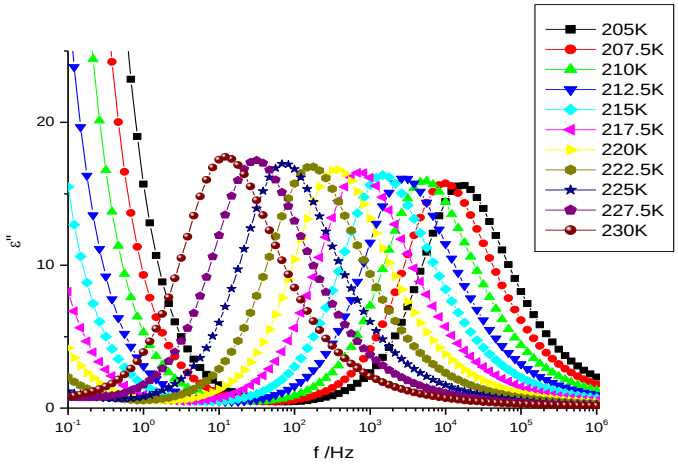

Figure 4.1: Experimental results (symbols) for the low field dielectric loss spectrum of glycerol from T= 205-230K with steps of 2.5K.

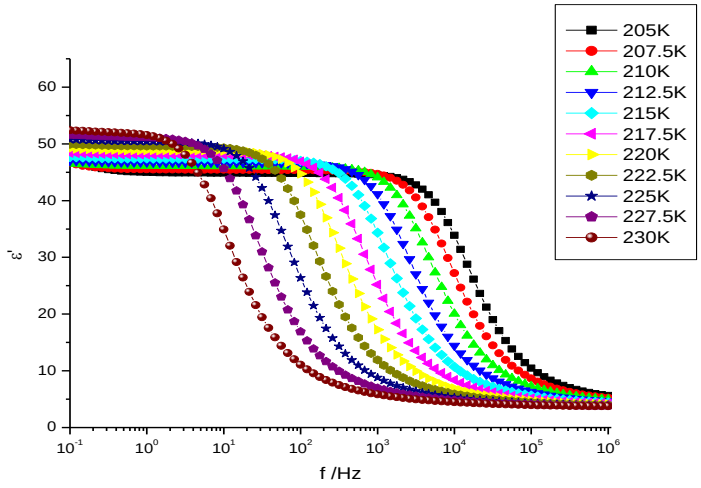

Figure 4.2: Experimental results (symbols) representing the spectrum for ε' of glycerol from T= 205-230K with steps of 2.5K.

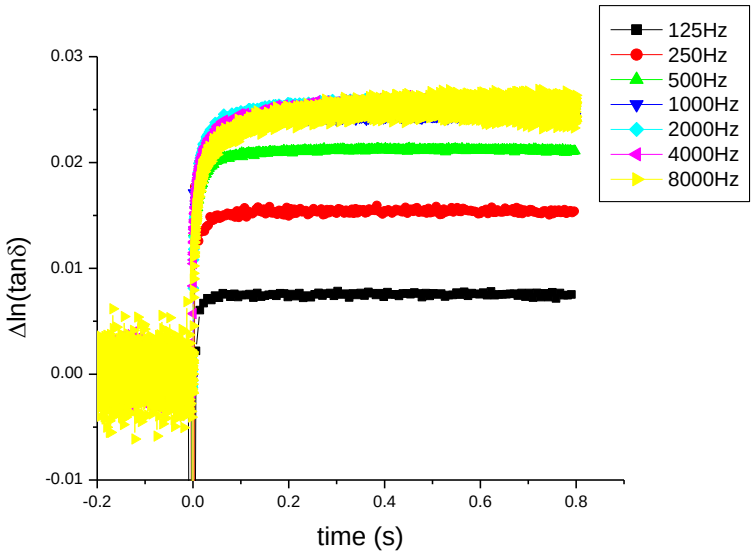

Figure 4.3: Experimental results for the time-resolved relative changes in the loss factor, $\tan\delta_{rel}$ using different frequencies for glycerol at T = 207K. The transition from low to high field occurs after 20% of the signal i.e. 0.2ms of the 1 sec signal with processing 1 million samples/sec.

With these results we investigated the magnitudes of changes regarding fictive and real temperatures in high field impedance measurements. It is shown that the sample thickness plays an important role, and fictive and real temperature effects can be discriminated experimentally. The experiments indicate that Joule heating and thermal diffusion to the electrodes can underestimate the increase in real temperature. This plays a role in describing its implications in microwave chemistry and heating via cell phone use.

The main material used for this study is the polar glass-forming liquid glycerol (99.5 + %, spectrophotometric grade), which has been used as received from Aldrich. The water concentration is 710±20 ppm, as determined previously using Karl Fischer titration [26].

The time resolved field effects have all been measured on glycerol at T=207K. For this situation, the spectra for dielectric loss ε" and loss factor tan δ are shown below

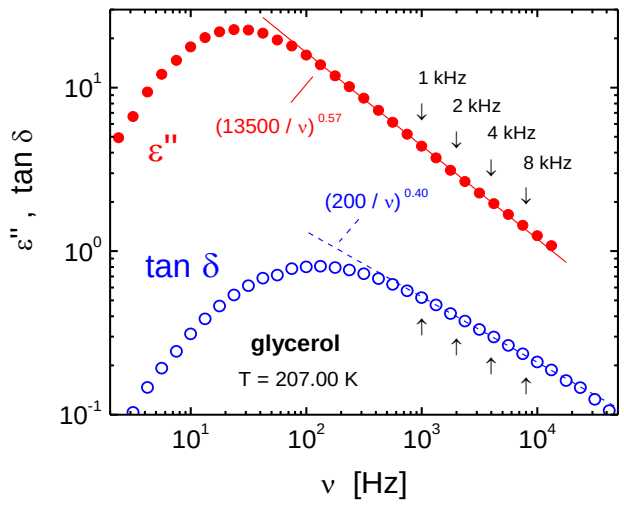

Figure 4.4: Dielectric loss (ε", solid symbols) and loss tangent (tanδ, open symbols) for glycerol at T =207K. The lines represent the power laws approximating the high frequency slopes, $\varepsilon'' = (13500/\nu)^{0.57}$ and $\tan\delta = (200/\nu)^{0.40}$. The arrows indicate the measurement frequency positions of the time resolved experiments.

This graph includes the frequency positions of the time resolved experiments which are indicated by arrows. A typical result of the time resolved field effect

experiment is depicted in Figure 4.5 where the upper data set represents the original values for tanδ as measured. This is a four point correlation function, two points in time regarding polarization (defined by the measurements frequency of 8kHz) , and two points in time regarding the onset of energy transfer (at t=0). Following earlier reasoning, we assume that the final linear increase of $\Delta \ln(tan\delta)$ with time is due to a temperature increase of the electrodes. In order to justify this, slope $S = d\Delta \ln(tan\delta)/dt$ is evaluated for times t≫0 for different frequencies ν, sample thickness d, and electric field amplitudes E_0. An example for a linear fit leading to such a slope is included as line Fig 4.5. For each case the power is evaluated, and Fig. 4.6 compiles the results S(P) from 22 separate measurements at two different nominal distances d = 10μm and 25μm.

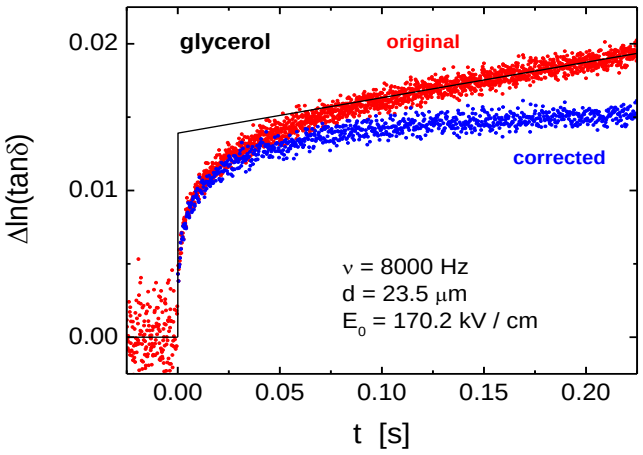

Figure 4.5: Time-resolved field induced relative change of the loss tangent, $\Delta \ln(tan\delta) = \Delta tan\delta/tan\delta$ for glycerol at T= 207K measured at ν = 8kHz. The electric field was increased from E_0 = 34 kV/cm to 170kV/cm at t=0 by increasing the voltage across d=23.5μm sample by a factor of 5. The upper data set labeled

'original' is as measured and displays a constant slope for t>0.1 s. The lower data is corrected for this temperature drift of the electrodes via subtracting the linear fit, y = H + Sx, represented by the solid line, for t>0.

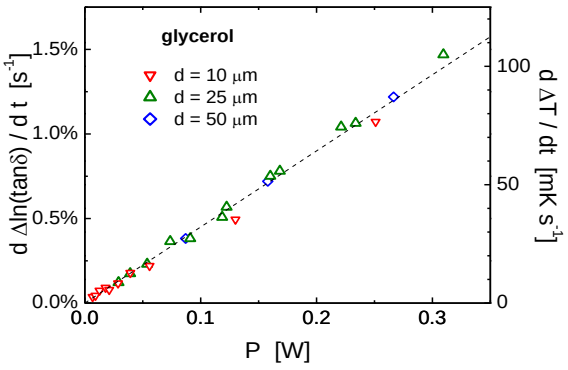

Fig. 4.6: Slopes $S = d\Delta \ln(tan\delta)/dt$ as indicated in Fig 4.4 versus powerP for different samples of glycerol at T= 207K. Power levels in the range of 6.7 to 310 mW have been achieved by varying electrode distances (10 to 50 μm), frequency (1 to 8 kHz), and electric fields (57 to 270 kV/cm). The dashes line reflects a fit $dT/dt = p/C_p$ with C_p = 3.1J/K.

With the long time slopes S evaluated, the linear relation S x t for t>0 is subtracted from the time resolved $\Delta \ln(tan\delta)$ data, resulting in curves that become level at long times. Figure 4.5 displays an example of this correction (lower data), now equivalent to the situation of isothermal electrodes. By averaging over the long time values of these corrected curves, we obtain the steady state field induced change tanδ under constant electrode temperature conditions. These heights are compiled below in Figure 4.7

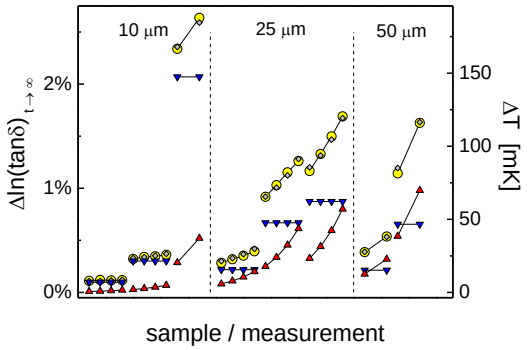

Figure 4.7: Experimental results (circles filled yellow) for the steady state field induced relative change of tanδ, derived from the time resolved curves after correcting for the electrode temperature drift. The abscissa serves only to separate distinct measurements, which are separated in terms of the nominal electrode distance d, as indicated. For each d, data are sorted by the field amplitude E_0. Values with a common d and E_0 are connected by lines and differ only in the frequency ν. Within each connected set, points are uniformly spaced along the abscissa regarding log(ν). The calculated fictive and real temperature effects are shown as triangles pointing down (blue) and up (red) respectively. The sum of these two effects is represented by small diamonds (grey).

Heating a dielectric by time dependent fields tends to generate fictive temperatures of the absorbing modes that are elevated above the true bath temperature. The net temperature effects are studied by time-resolved high field dielectric relaxation experiment that allows us to quantify the changes of the configurational, real sample, and electrode temperatures. The results demonstrate that the impact of 'configurational heating' is significant only for low frequencies of the electric field and samples that are thermally clamped to a thermostat (metal

electrodes) in a very effective manner. For heating macroscopic samples with fields in the microwave frequency range, we conclude that any disparities between configurational and real bath temperature are negligible, unless a mode is involved that can absorb energy at a rate much faster than its equilibration with the bath. The non-equilibrium effects of fictive temperatures that exceed the real temperature do not seem important in the context of microwave heating. This allows us to understand the difference between conventional and microwave heating and the effects of cell phone radiation on tissue material.

4.2 Monohydroxy Alcohols

Time-resolved techniques are used to quantify the non-thermal effects of energy absorption for simple and associating polar liquids in their supercooled state. Experiments performed in a low-frequency range tracks the flow of energy in time on slow degrees of freedom and transfers to the vibrational heat bath of the liquid, as is the case for microwave heating. We know that monohydroxy alcohols behave differently than simple non-associating liquids due to their distinct origins of the prominent dielectric absorption mode for the two classes of liquids. Monohydroxy alcohols have very small changes to explain its analogy to microwave chemistry due to observed nonthermal effects that are accelerated without increasing sample temperature. The dynamic behavior of faster relaxation time constants adjust to temperature hence the modes of the dispersive α-relaxation are separated into a ‘relaxation’ and an ‘aging’ regime explaining the incompatibility of heterogeneous dynamics with physical aging observations.

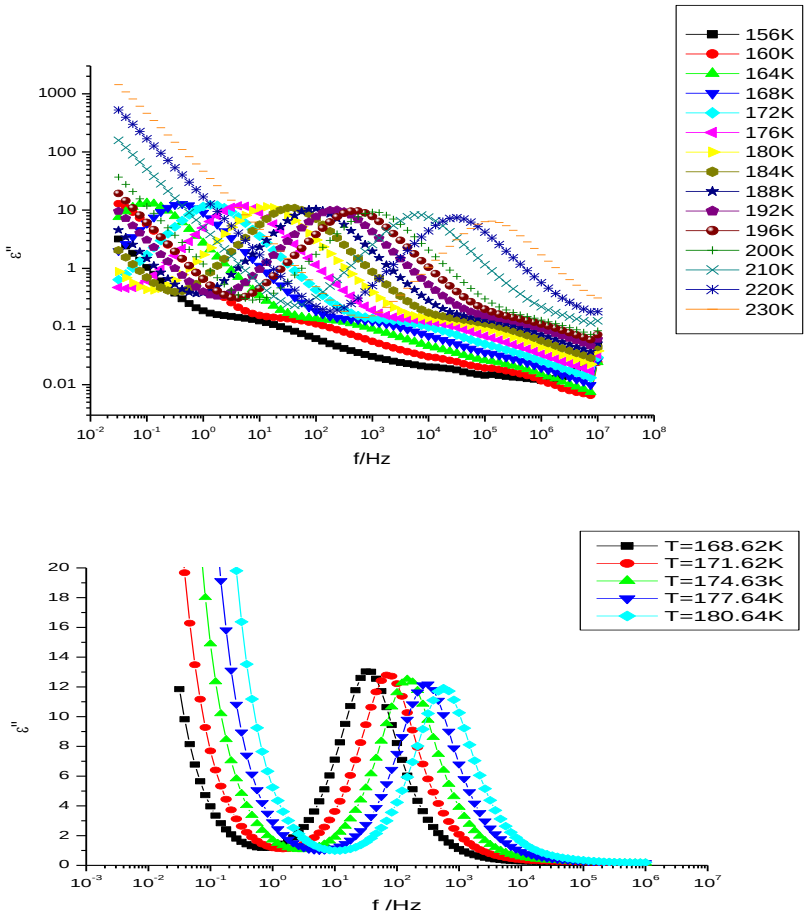

Figure 4.8: Experimental results (symbols) for the low field dielectric loss spectrum of 2-ethyl 1-hexanol from T = 156-230K with steps of 4K from 156-200K and steps of 10K from 200-230K (left), and 2-ethyl-1-butanol from T = 168 – 180K with steps of 3K (right).

For this case the modes which absorb energy are associated with structural relaxation, dipolar orientation, or conductivity but are not vibrational in nature. Microwave energy is not transferred to the slow degrees of freedom by acquiring energy prior to releasing to the vibrational modes. Approximately one-half of the total equilibrium heat capacity of the liquid is associated with slow degrees of

freedom. A sinusoidal field is applied to measure the frequency resolved dielectric property by impedance technique with very small fields.

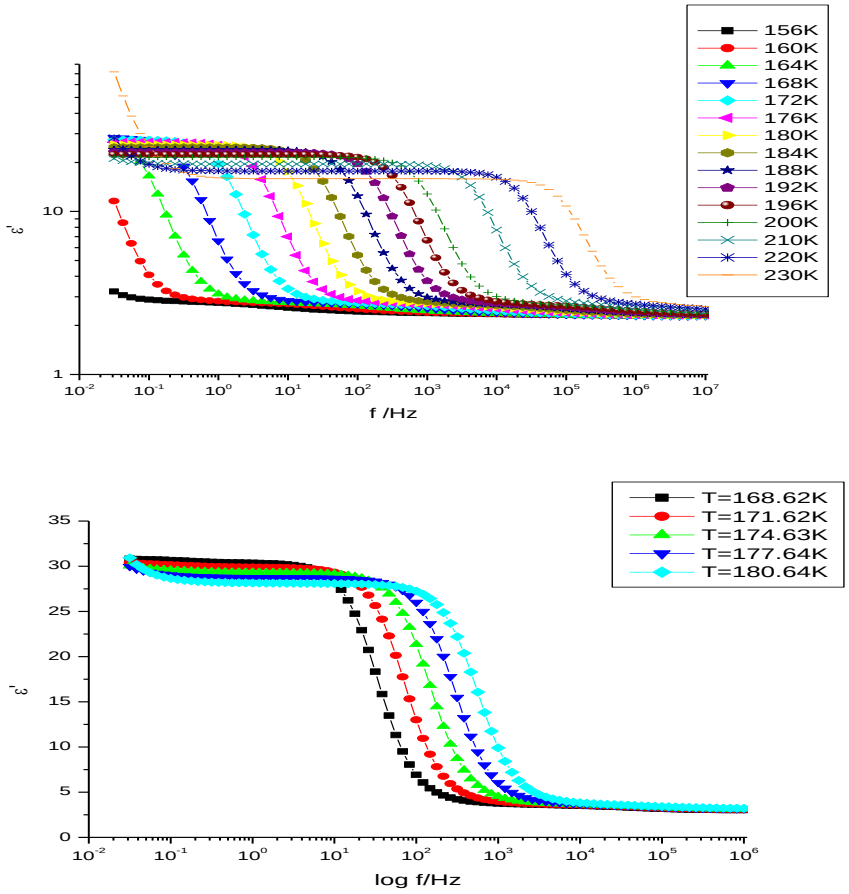

Figure 4.9: Experimental results (symbols) representing the spectrum for ε' for 2-ethyl-1-hexanol from T = 156-230K with steps of 4K from 156-200K and steps of 10K from 200-230K, and 2-ethyl-1-butanol from T = 168 – 180K with steps of 3K (right).

Our goal here is to use time-dependent field for irreversibly transferring energy from the electric field to the sample as done for dielectric hole-burning.

Depending upon the liquids used, response depends upon the amplitude of the electric field to drive it beyond the linear regime. Liquid used here are 2-ethyl-1-hexanol (2E1H, 99.6%) and 2-ethyl-1-butanol (2E1B, 98%) purchased from Aldrich and used as received.

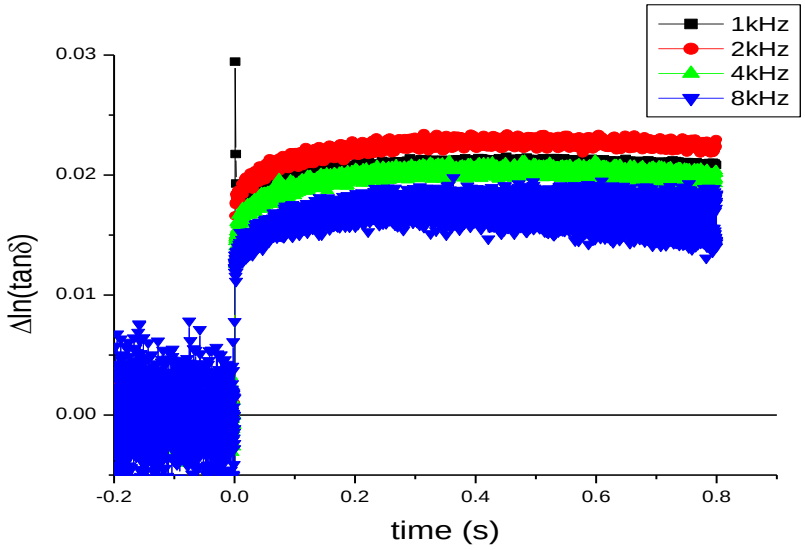

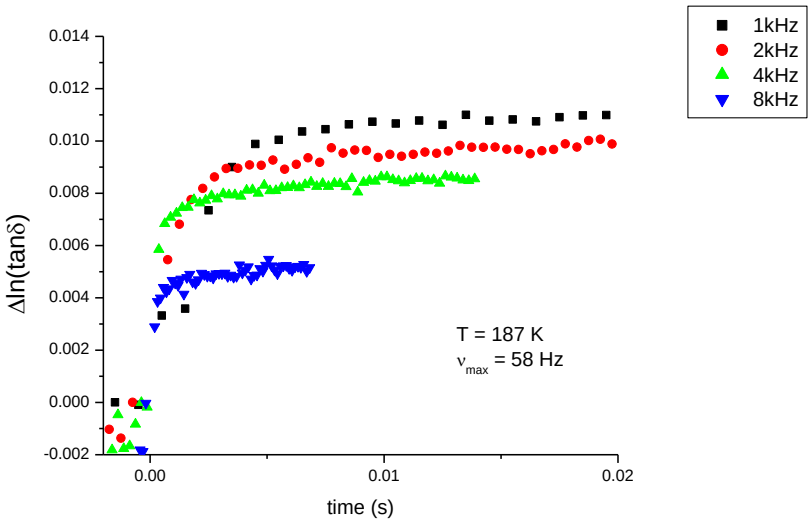

Figure 4.10: Experimental results (symbols) for the time-resolved changes in the loss factor $\tan\delta_{rel}$, using four different frequencies ν = 1000, 2000, 4000 and 8000 Hz for 2-ethyl-1-hexanol at T=187K. The transition from low (80 kV/cm) to a high (400 kV/cm) field occurs. Field transition occurs after 8 periods for the graph on the bottom (waveform modulation) and high field is applied for 56 periods while the sample is equilibrated at zero field for times νt<-200ms for the graph on the top (arbitrary amplitude modulation).

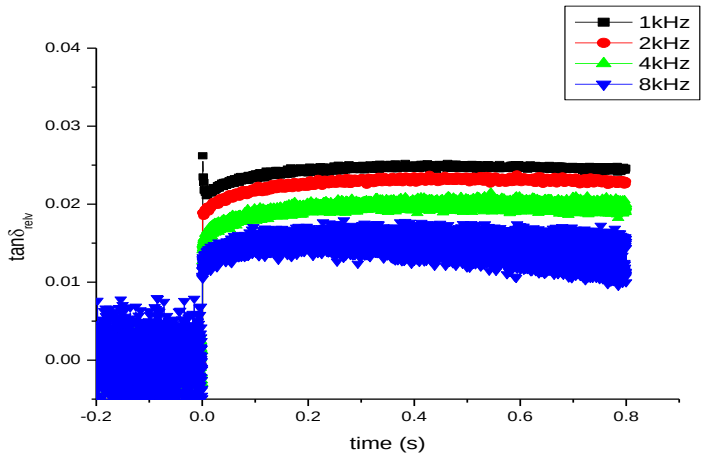

Figure 4.11: Experimental results (symbols) for the time-resolved changes in the loss factor $\tan\delta_{rel}$, using four different frequencies ν = 1000, 2000, 4000 and 8000 Hz for 2-ethyl-1-butanol at T=171K. The transition from low (80 kV/cm) to a high (400 kV/cm) field occurs. The sample is equilibrated at zero field for times νt<-200ms for the graph on the left (arbitrary amplitude modulation).

As we can see above the percentage change is loss factor tanδ varies from 2% for amplitude modulation for the monohydroxy alcohols used to around 1% for waveform modulation. This led us to postulate that the difference in change of

loss factor is due to the out of phase amplitude transition which does not coincide with the beginning of the period and hence plays a significant role in amplification of non-linear component. The relaxation times were studied according to the non-exponential function for the loss factor $\tan\delta_{rel}$

$$Y = A + B(1- e^{-\frac{t}{\tau}})^{\beta} \quad (4.1)$$

where Y represents the recorded response of the loss factor, A is the rising point of the configurational temperature or the irreversible energy transfer into the system and B is the heat dissipated into the system as real temperature rise.

The relaxation times were measured over a wide temperature range as shown in Figure 4.12 but no significant temperature and frequency dependence in the relaxation patterns of the modes was observed.

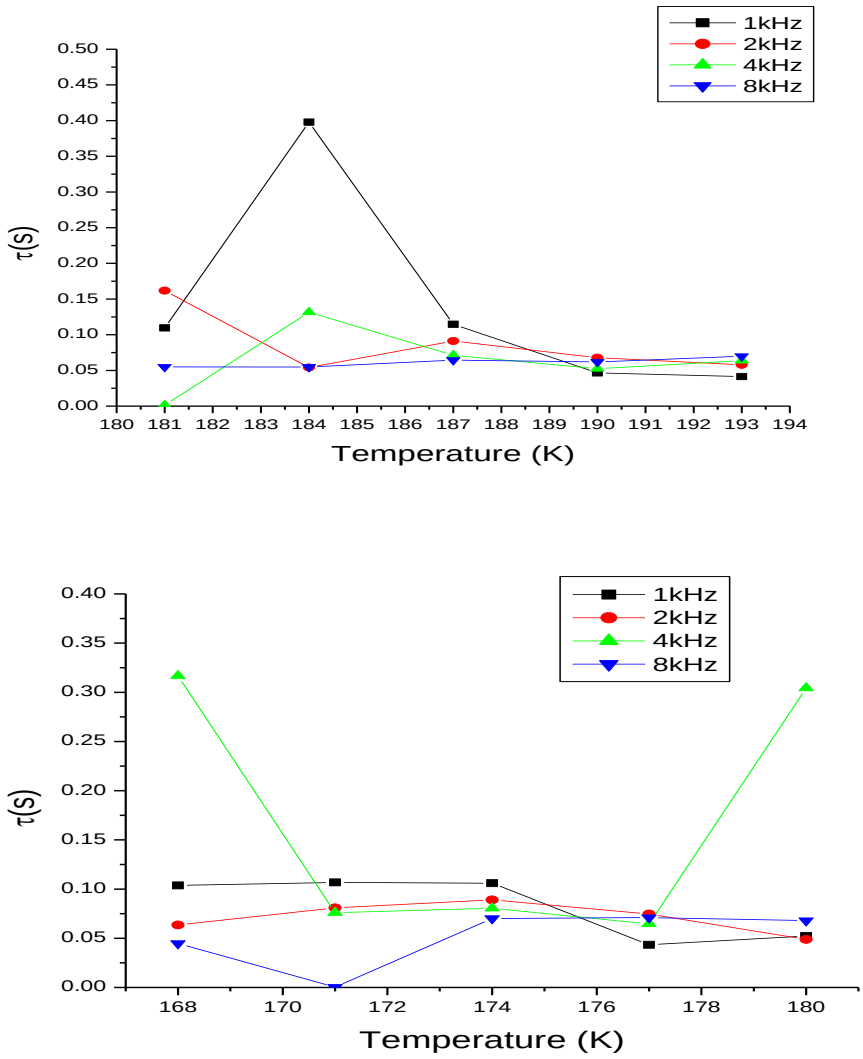

Figure 4.12: Experimental results (symbols) for the relaxation times τ vs temperature for 2-ethyl-1-hexanol (left) and 2-ethyl-1-butanol (right) for frequencies ranging from ν = 1-8 kHz.

The study reflected that due to typical behavior of monohydroxy alcohols the energy absorbed by the slow degree of freedom is dependent on the power to a very feeble extent. The out of phase component of the amplitude transition does not play a role in reflecting this behavior a shown in Figure 4.13 below where

amplitude modulation and waveform modulation were studied for 2-ethyl-1-hexanol. The waveform modulation was programmed to apply the high field not at the beginning of the wave which would present an out of phase transition for waveform modulation as is the case for arbitrary amplitude modulation. It was observed that the loss factor tanδ does not depend on the number of cycles to reflect the configurational temperature rise and is independent of the point of phase transition. The amplitude transition does not occur at the starting of the wave but the effect disappears within initial cycles of modulation. Hence it is the behavior of these alcohols which shows relaxation times independent of frequency and temperature. The temperature rise causes the relaxation modes to relax faster than in the more viscous regime i.e. at lower temperatures. But even at these higher temperatures no particular pattern was observed with frequency showing the faster modes need not necessarily have faster heat dissipation as compared to the slower modes signifying that monohydroxy alcohols have a varying trend in absorbing heat and dissipating it.

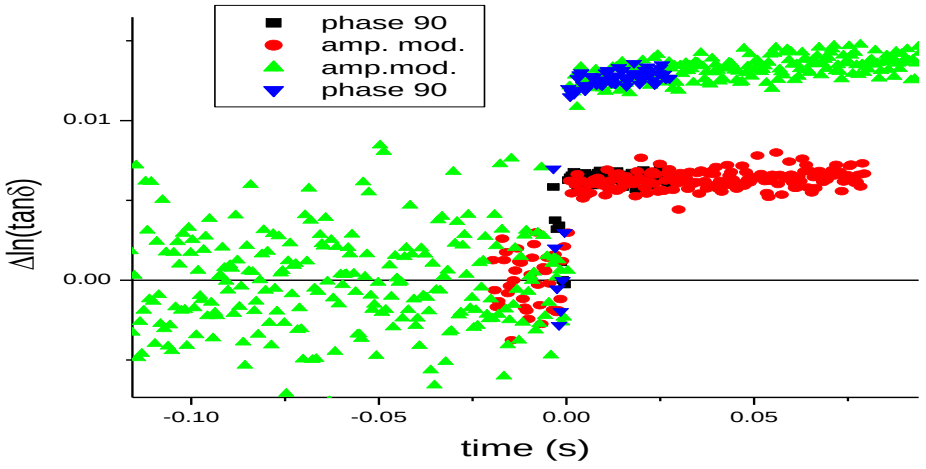

Figure 4.13: Experimental results (symbols) for the time-resolved changes in the loss factor $\tan\delta_{rel}$, using ν = 4kHz for 2-ethyl-1-hexanol at T=181K. The transition from low (56.6 kV/cm) to a high (283 kV/cm) field occurs red and black for arbitrary amplitude and waveform modulation respectively. The transition from low (80 kV/cm) to a high (400 kV/cm) field occurs green and blue for arbitrary amplitude and waveform modulation respectively.

4.3 Microemulsion

We focus on a study related to 'water-in-oil' type microemulsion. The three component systems used are propylene glycol (PG, 1,2-propanediol) as the polar or "water" phase and decalin (DHN, decahydro-napthalene) as the nonpolar or "oil" phase. The glass transition temperatures of the liquids are T_g = 167K for PG and T_g = 135K for DHN which are immiscible without a surfactant. As a surfactant for reverse miscelles AOT (aerosol OT, sodium bis(2-ethylhexyl)sulfosuccinate) is used. Using the techniques the regime of stable and optically clear microemulsions within the phase diagram of this ternary system as is used [27-28]. Stability was found in a range even when sample was cooled to 77K. The composition used for our study found by the phase diagram was 10.2% PG, 36.1% AOT and 53.7% DHN (by weight). PG being a dielectrically active liquid was studied and the dynamics was observed when confined in these reverse micelles.

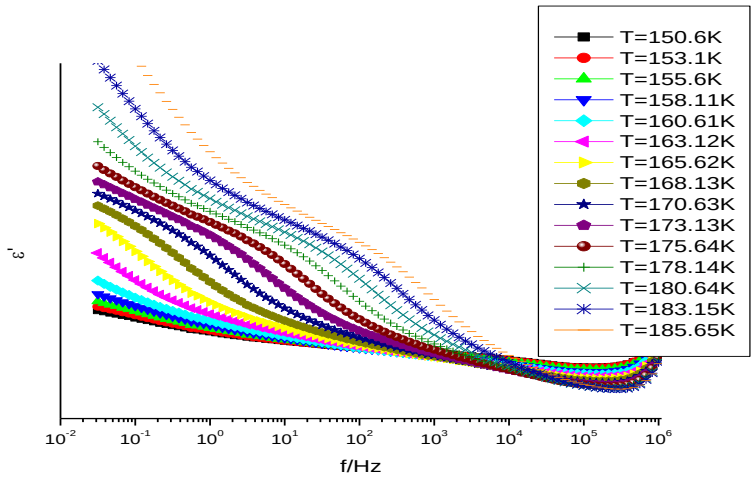

Figure 4.14: Experimental results (symbols) representing the spectrum for real part ε'(ω) for PG/AOT/decalin microemulsion from T = 150-185.5 K with steps of 2.5 K for 10.2% by wt. PG.

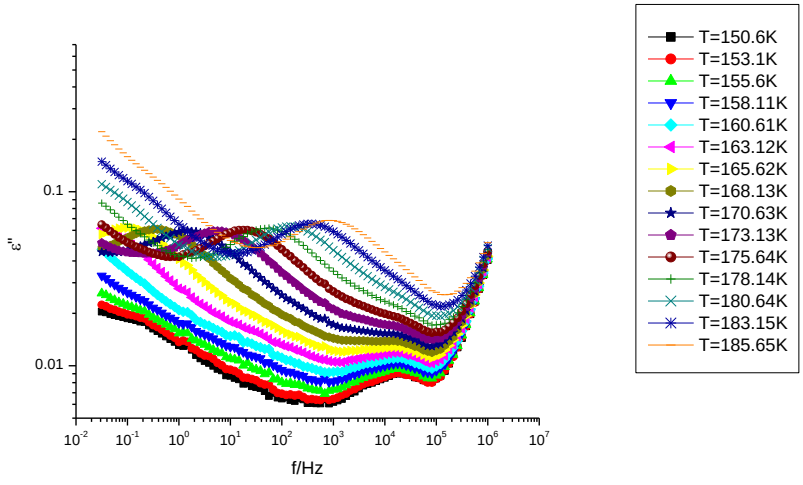

Figure 4.15: Experimental results (symbols) for the low field dielectric loss spectrum of PG/AOT/decalin from T = 150-185.5 K with steps of 2.5 K for 10.2% by wt. PG.

The application of electric field causes the vibrational modes of the polar molecule Propylene Glycol (PG) to relax without affecting the non-polar decalin molecules. Figure 4.16 and 4.17 shows the energy dissipated into the polar molecules of the microemulsion on the timescale of the pure PG molecule. The proportion of PG in the microemulsion is signified by the relaxation pattern of the slow modes which is reduced by a factor of 1/10 th as compared to the pure PG molecule. The energy dissipated is plotted against the square of the field and we know that power delivered varies with square of the field therefore the microemulsion graph is scaled by a factor of 3.2 i.e. square root of 10. This is according to the theory that when a varying electric field is applied the vibrational modes absorbing energy are of the polar molecules and the non-polar molecule does not play a significant role in altering the effective field on the former.

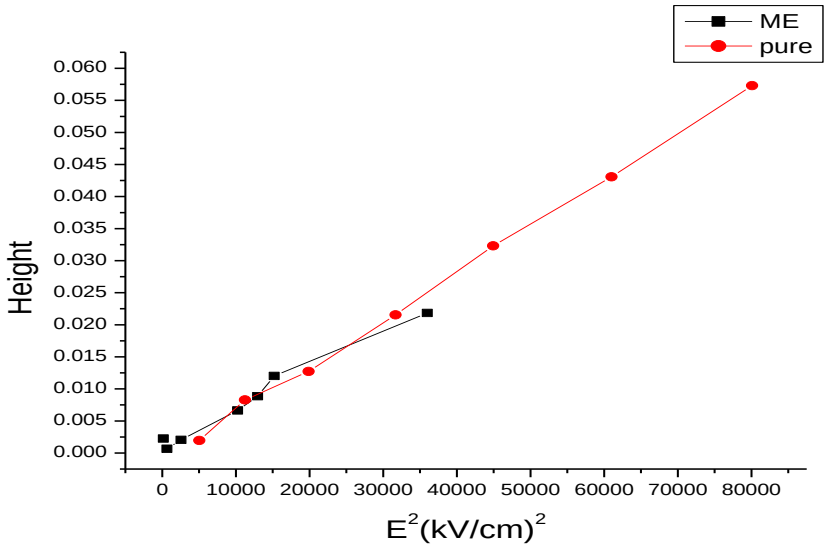

Figure 4.16: Experimental results(symbols) representing energy dissipated in the PG/AOT/decalin microemulsion (ME) for 10.2% by wt. PG. at T= 175K as compared to pure Propylene Glycol (PG) scaled by a factor of 10 vs Field^2 for ME.

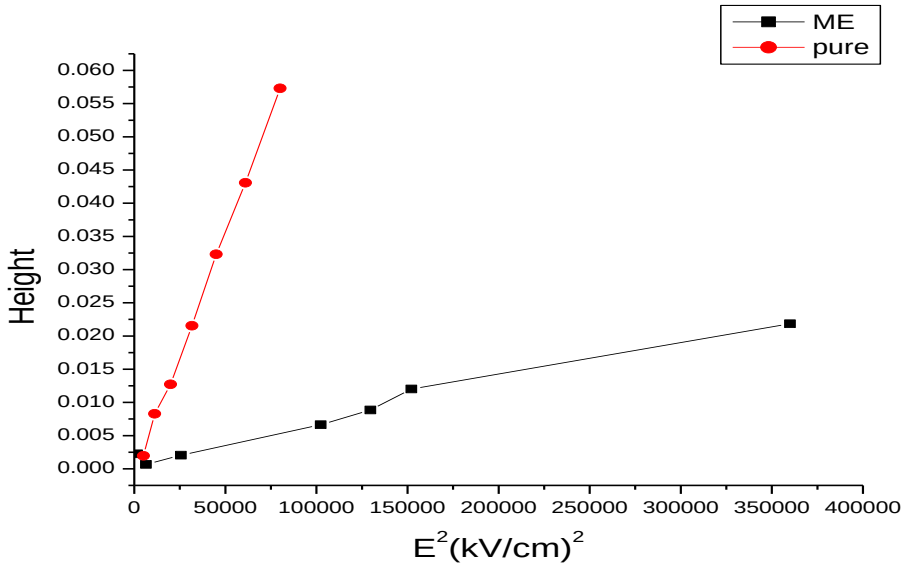

Figure 4.17: Experimental results(symbols) representing energy dissipated in the PG/AOT/decalin microemulsion (ME) for 10.2% by wt. PG. at T =175K as compared to pure Propylene Glycol (PG).

From the phase diagram of the mentioned microemulsion [29] the regime of microemulsion can be extended to 5.1% wt. of PG and increasing the decalin content by 5.1% by wt. which will help us postulate the linear effect of effective field on polar molecules.

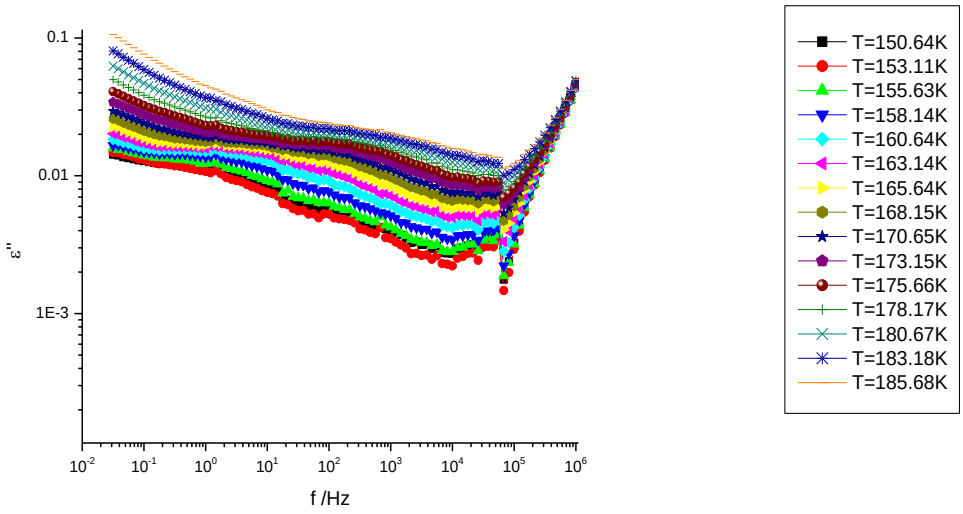

Figure 4.18: Experimental results (symbols) for the low field dielectric loss spectrum of PG/AOT/decalin from T = 150-185.5 K with steps of 2.5 K for 5.1% by wt. PG.

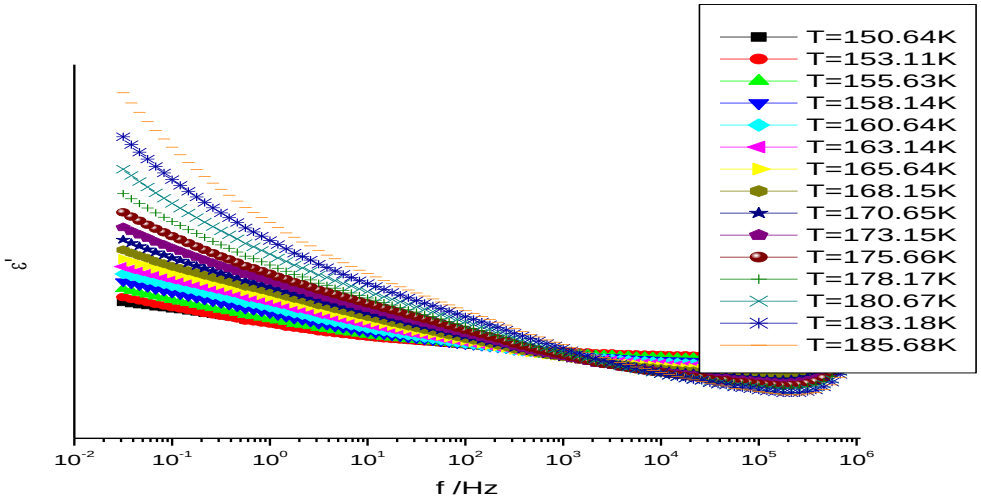

Figure 4.19: Experimental results (symbols) representing the spectrum for real part ε'(ω) for PG/AOT/decalin microemulsion from T = 150-185.5 K with steps of 2.5 K for 5.1% by wt. PG.

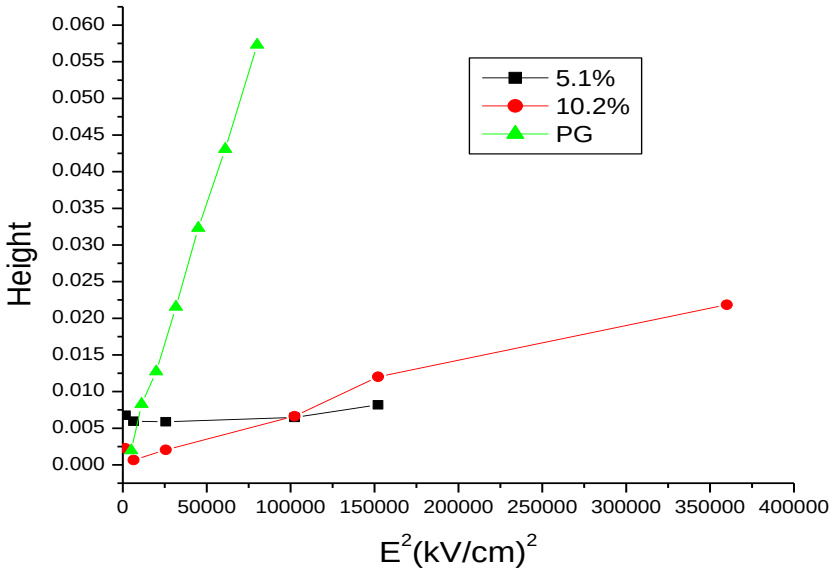

Figure 4.20: Experimental results(symbols) representing energy dissipated in the PG/AOT/decalin microemulsion (ME) for 5.1% by wt. PG. as compared to 10.2% by wt. PG in ME and pure Propylene Glycol (PG).

Figure 4.20 signifies that the enrgy dissipated in 5.1% by wt. of PG in the microemulsion is not proportional to the presence of polar molecules. The scrutiny of varying composition of microemulsion represents the non-linesr effects of the non-polar molecule. The effective field is altered by the presence of non-polar molecule surrounding the polar part which gives rise to non-thermal effects in the microemulsion. The reverse micelles alter the relaxation pattern of the polar molecule, Propylene Glycol (PG). We observed that the presence of

non-polar molecule around polar molecule in small particle regime affects the effective field and hence the energy transferred to the molecule as configurational temperature rise contrary to the actual temperature rise.

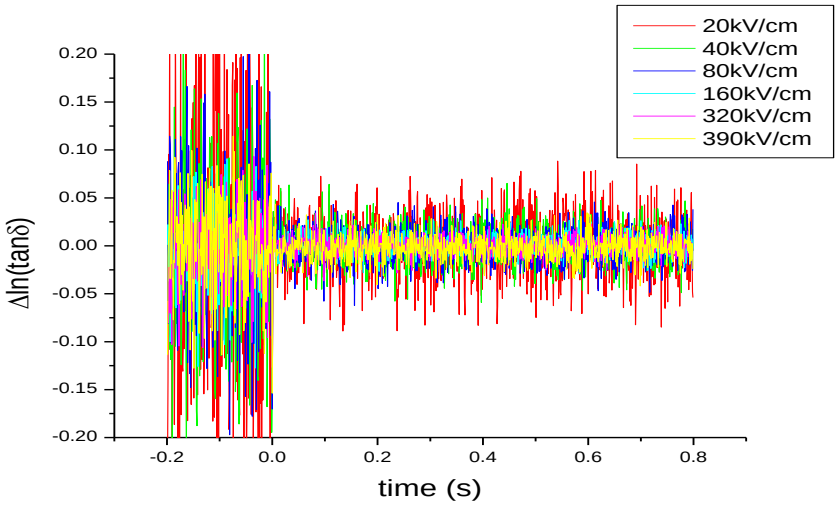

Figure 4.21: Experimental results (symbols) for the time-resolved changes in the loss factor $\tan\delta_{rel}$, using six different fields for the frequency ν = 1000 Hz for 5.1% by wt. PG in ME at T=171K. The graph reflects that due to the presence of non-polar molecule the percentage increase in loss factor is not significant in the range of 20kV/cm to 390kV/cm. The sample is equilibrated at zero field for times νt<-200ms for the graph (arbitrary amplitude modulation).

4.4 Thin Film

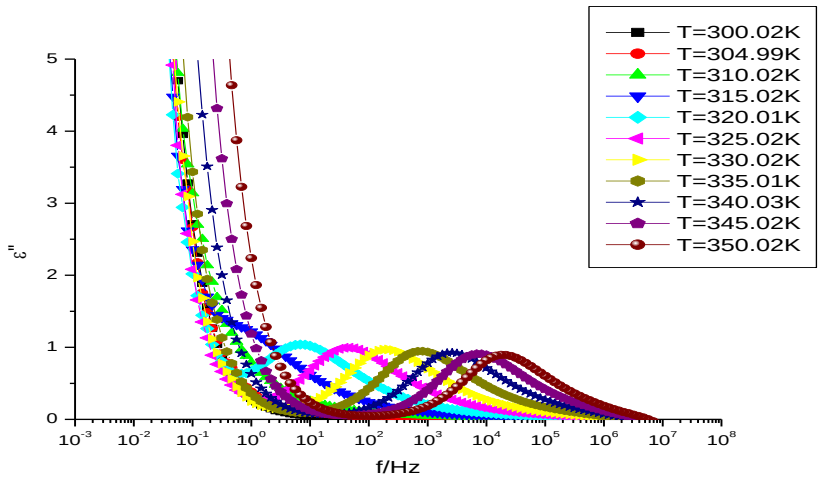

Figure 4.22: Experimental results (symbols) representing the spectrum for loss factor ε”(ω) for the thin film of Poly Vinyl Acetate (PVAc) from T = 300-350 K with steps of 5 K.

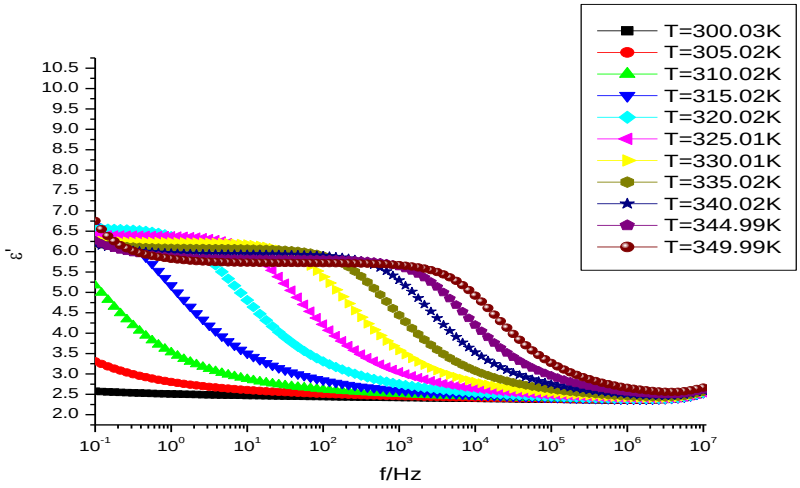

Figure 4.23: Experimental results (symbols) representing the spectrum for real part ε’(ω) for the thin film of Poly Vinyl Acetate (PVAc) from T = 300-350 K with steps of 5 K.

A thin film was prepared from Poly (vinyl acetate), Average M_w ca. 12800 (GPC) purchased from Aldrich and was used as received. A 10 micron Teflon spacer was used to reduce the edge effects on brass plates with 20mm diameter and 14mm diameter for the bottom and top plates respectively. The thinfilm was found to be stable and robust for high-fields, 566 kV/cm as shown in Fig. 4.24. The long chain polymers have a typical characteristic of crystallizing near T_g or showing very small increase in loss factors by the increase of electric field due to intramolecular bonding between the molecules altering the relaxation patterns of the slow modes.

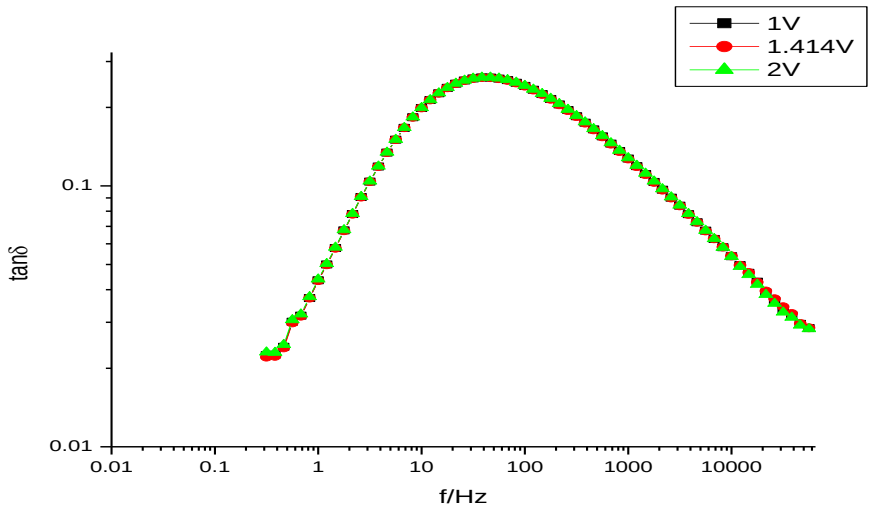

Figure 4.24: Experimental result (symbols) showing tanδ spectrum for fields of 283, 400 and 566 kV/cm for the thin film of Poly Vinyl Acetate (PVAc).

The relaxation pattern is unaltered for high fields. High-field application will provide energy to the slow modes of the polymer and accordingly reduce the noise factor by increasing the field.

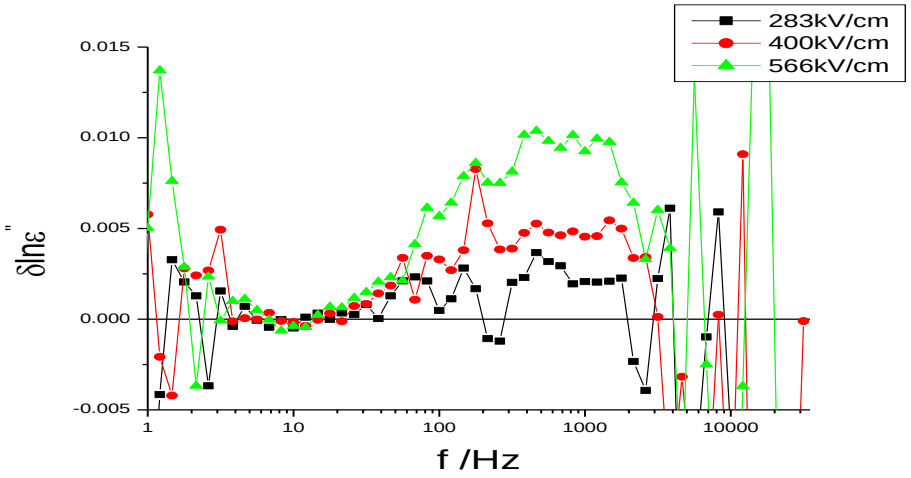

Figure 4.25: Experimental results (symbols) for the field induced relative change in the loss, δlnε" vs frequency f for Poly (vinyl acetate) thin film at T=323 K. The curves are recorded at different fields E_0 as indicated and evaluated relative to a low field reference using E_0=40 kV/cm.

The loss factor as shown in Fig. 4.25 displays a non-linear behavior in the dynamics of the relaxation pattern of the film. This non-linear effect is predominant in the low frequency region of 1000 Hz displaying a significant decrease in loss factor irrespective of the field applied. The dynamics of long chain polymers has not been studied in much detail. The non-linear behavior occurring in the same low frequency range for all the fields applied generates a

hypothesis that this could be due to the behavior of the polymer or can be due to the operational amplifier.

To further test this theory the same experiment was conducted on Glycerol and the results displayed a significant change in the non-linear effects. Various configurations of operational amplifier setup is used to test the validity of the postulation. Two different amplification factors of 200 and 100 were used with Trek model 700 and Trek PZD model 350A amplifiers respectively in connection with the operational amplifier to show the changes in loss factor for glycerol as seen in Fig. 4.26.

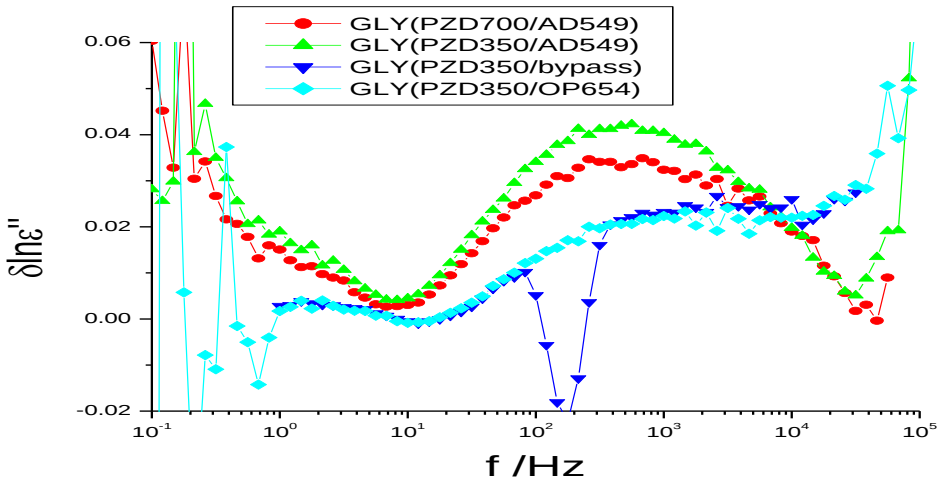

Figure 4.26: Experimental results (symbols) for the field induced relative change in the loss, δlnε" vs frequency f for Glycerol at T=207 K. The curves are recorded at different fields E_0 as indicated and evaluated relative to a low field reference using E_0=40 kV/cm. The number (100) and (200) signifies the amplification factor of the amplifier used in combination with different orientations of the operational amplifier.

The result shows the decrease of non-linear effect of the thin film due to use of amplifier without the AD-549L operational amplifier. This was in accordance to our postulation of presence of non-linear effects due to the amplifier. This was corrected for by using a different operational amplifier hereby increasing the transit frequency of the amplifier from 26750 Hz to 800 kHz. The results presented in Fig. 4.27 signify the corrected behavior of the operational amplifier hence a significant decrease at 1 kHz is no longer observed. The loss factor increases after the peak frequency at the specified temperature and maintains the constant loss which contributes to the actual temperature rise of the sample.

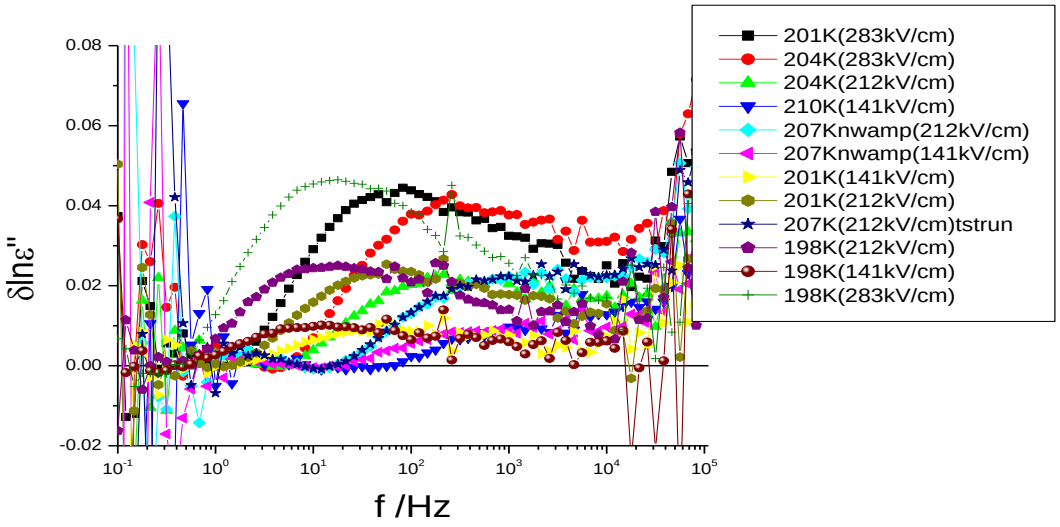

Figure 4.27: Experimental results (symbols) for the field induced relative change in the loss, δlnε" vs frequency f for Glycerol at T=207 K. The curves are recorded at different fields E_0 and temperatures as indicated and evaluated relative to a low field reference using E_0=40 kV/cm.

The corrected effects for the thin film of Poly (vinyl acetate) was observed in Fig. 4.28 at 323K for 4 different fields of 283, 340, 400 and 500 kV/cm which as compared to Fig. 4.25 does not show a non-linear effect after a threshold frequency signifying a loss factor of 1-2% in the polymer. This effect can be used to study the insulation effects and the configurational rise in temperature in these long chain molecules which are robust through varying high-fields.

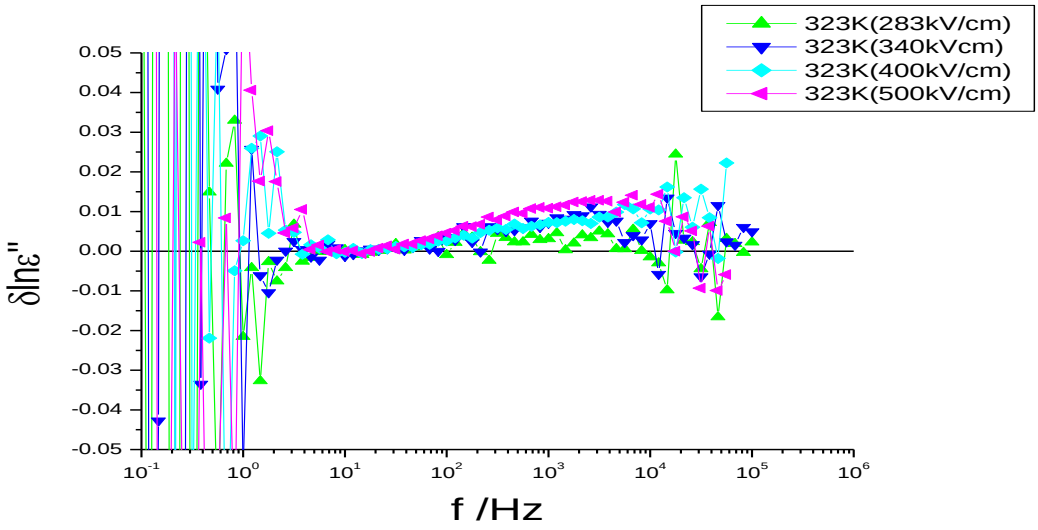

Figure 4.28: Experimental results (symbols) for the field induced relative change in the loss, δlnε" vs frequency f for Poly (vinyl acetate) at T=323 K. The curves are recorded at different fields E_0 as indicated and evaluated relative to a low field reference using E_0=40 kV/cm.

Chapter 5

CONCLUSION

We see that application of electric field causes the slow degree of freedom to absorb energy. This energy is translated into the configurational, sample and electrode heating. High-field time-resolved experiments performed in the range of 10 mHz to 10MHz result in the non-linear behavior of the molecules, which is analogous to microwave heating. The distinct domains are dynamically distinct each characterized by different time constants which determine the dielectric and thermal relaxation time. Heterogeneity dynamics is studied and the model is in affirmation for different compounds. The extent of configurational temperature rise as compared to the real vibrational temperature, frequency dependence and dissipative energy changes by the addition and removal of high field have been studied. Glycerol shows good agreement with the model and presenting that in microwave heating the thickness of the sample does not play a significant role in temperature rise due to the varying behavior of real and configurational temperature rise for samples above 10μm. Behavior of monohydroxy alcohols was confirmed by the varying relaxation timescales independent of frequency and temperature. The structural relaxation time is found to be shorter than prominent dielectric mode that absorbs the energy. They are known to be different from simple non-associating fluids due to their dominant primary relaxation patterns. The non-thermal effects are suppressed due to loss of calorimetric mode in spectral range sustaining configurational energies. The hydrogen bonding studies of this category of alcohols is still a mystery due to presence of one hydroxyl

group. Variation in hydrogen bonding reflects different mechanisms and structural relaxation.

Propylene Glycol having a dielectric constant of 37 absorbs energy on a higher magnitude as compared to the nanodroplets suspended in a non-polar liquid. The studies show that effective field applied on the polar molecule is not equivalent to the external field applied. The modes absorbing energy are of the polar molecule but the non-polar part plays a significant role in reverse micelle structure. This was confirmed for 5.1% and 10.2% by weight of Propylene Glycol in the microemulsion.

Polymers have shown significant loss factor by the application of high field even resisting fields of 566 kV/cm. These show a significant potential for use in insulation and pharmaceutical purposes. The non-linear effect of the operational amplifier was corrected for signifying a better fit to the model for high field measurements showing a constant loss even in the high frequency range.

Future work is to study the behavior of hydrogen bonding in monohydroxy alcohols and to understand them better. These alcohols are used for various commercial purposes i.e. pharmaceutical, disinfectants, food and agricultural products and also help in understanding the most important liquid i.e. water for us. More detailed study is to be conducted regarding insulation properties for long chain polymers and to study their robustness. These significant changes in the loss factor present a potential application for high-voltage application of these polymers thin films. The thin films can be used for insulation in a temperature

range of up to 60^0C due to their high glass transition temperature and stability across a considerable range in T.

REFERENCES

[1] *Dielectric Relaxation in Solids*, A. K. Jonscher, *J. Phys. D: Appl. Phys.* **32** R57 (1999).

[2] *Broadband Dielectric Spectroscopy*, F. Kremer, A. Schonhals, Springer (2003).

[3] *Principles of Dielectrics*, B. K. P. Scaiffe, Oxford Press (1989).

[4] R. Richert, J. Phys.: Condens. Matter 14 (2002) R703 - R738.

[5] A. Khalife, U. Pathak, R. Richert, Eur. Phys. J. B 83 (2011) 429 – 435.

[6] *Analog Devices, Datasheet for AD549, rev*. F (2006), p. 13

[7] R. Kubo, J. Phys. Soc. Jpn. 12, 570 (1957).

[8] B. Schiener, R. Bo¨hmer, A. Loidl, and R.V. Chamberlin, Science 274, 752 (1996).

[9] R.V. Chamberlin, B. Schiener, and R. Bo¨hmer, Mater. Res. Soc. Symp. Proc. 455, 117 (1997).

[10] B. Schiener, R.V. Chamberlin, G. Diezemann, and R. Bo¨hmer, J. Chem. Phys. 107, 7746 (1997).

[11] R. Richert, S. Weinstein, Phys. Rev. Lett. 97, 095703 (2006).

[12] K.Schro¨ter and E. Donth, J. Chem. Phys. 113, 9101 (2000)

[13] B. Schiener, R. B¨ohmer, A. Loidl, R.V. Chamberlin, Science 274, 752 (1996)

[14] R. Richert, S. Weinstein, Phys. Rev. Lett. 97, 095703 (2006)

[15] J. Malecki, J. Mol. Struct. 436-437, 595 (1997)

[16] C. Brun, C. Crauste-Thibierge, F. Ladieu, D. L'Hˆote, J.Chem. Phys. 134, 194507 (2011)

[17] A. Piekara, A. Chelkowski, J. Chem. Phys. 25, 794 (1956)

[18] B. Schiener, R.V. Chamberlin, G. Diezemann, R. B¨ohmer, J. Chem. Phys. 107, 7746 (1997)

[19] A. Piekara, A. Chelkowski, J. Chem. Phys. 25, 794 (1956)

[20] K.R. Jeffrey, R. Richert, K. Duvvuri, J. Chem. Phys. 119, 6150 (2003)

[21] R. Richert, R. B¨ohmer, Phys. Rev. Lett. 83, 4337 (1999)

[22] C. Crauste-Thibierge, C. Brun, F. Ladieu, D. L'Hˆote,G. Biroli, J.-P. Bouchaud, Phys. Rev. Lett. 104, 165703(2010)

[23] R. Richert, J. Non-Cryst. Solids 357 (2011)

[24] C. Hansen, F. Stickel, T. Berger, R. Richert, E.W. Fischer, J. Chem. Phys. 107, 1086 (1997)

[25] R. Böhmer, K.L. Ngai, C.A. Angell, D.J. Plazek, J. Chem. Phys. 99, 4201 (1993)

[26] R. Richert, J. Chem. Phys. 133, 074502 (2010).

[27] M. Kotlarchyk, S.-H. Chen, J. S. Huang, and M. W. Kim, Phys. Rev. Lett. **53**, 941 (1984).

[28] L.M. Wang, F. He, R. Richert, Phys. Rev. Lett. 92, 095701(2004).

[29] L.M. Wang, R. Richert, Phys. Rev. Lett. 92, 095701 (2004).